EUMETSAT

GOME-2 PMD Band Definitions 3.0 and PMD Calibration

Doc.No. : EUM/OPS-EPS/DOC/07/0601
Issue : v8
Date : 11 June 2010

EUMETSAT
Am Kavalleriesand 31, D-64295 Darmstadt, Germany
Tel: +49 6151 807-7
Fax: +49 6151 807 555 Telex: 419 320 metsat d
http://www.eumetsat.int

Table removed for internet publication

Document Change Record

Issue / Revision	*Date*	*DCN. No*	*Changed Pages / Paragraphs*
v1	05/11/2007		Initial draft version
v2	04/12/2007		Update after final test evaluations
v3 v3A	08/01/2008 11/01/2008		Complete revision after issuing of AR 9064 on PMD key-data for FM3
v4	21/01/2008		Evaluation of level 1B results for PPF 3.8 added
v5	09/05/2008		Results of PMD band test upload; New key-data concept for CHI, ALPHA, BETA GAMMA and ZETA New sections: Introduction; 5.2.7, Chapter 8 and 9.
v6	14/01/2009		Additional results from modelling ALPHA together with CHI
v7	01/07/2009		New Stokes fraction correction scheme based on TNO closed loop offline testing and results from PMD study group
v8	11/06/2010		Update for delivery of stray-light corrected key-data by TNO and update of dedicated chi for zeta for PMD key-data. Document has been re-structured to separate PMD band definition related issues from PMD calibration issues.

Table removed for internet publication

Table of Contents

1 INTRODUCTION

1.1 Purpose and Scope

This document describes the evolution of the on-board polarisation measurement device (PMD) band definitions [AD0] following an evaluation of the calibrated in-orbit data after about one year of operations including the intermediate one-day test-upload of a new set of definitions, based on GSAG recommendations, in October 2007 (v2.0) and after a complete revision of the spectral calibration for PMDs in February 2008 (v3.0).

The document describes our findings of problems in PMD key-data definitions for instrument version FM3 on Metop-A, which led to an additional revision of PMD band definitions, hereafter tagged as v3.0, as well as the issuing of a revised processor version.

The document describes the treatment of the remaining observed offsets in Stokes-fraction values in the viewing-angle, spectral and temporal domain.

The document also details additional updates to polarisation key-data relevant for PMD signal calibration quality and therefore subsequently relevant to the polarisation correction of main channel data. These updates have been implemented following joint investigations by EUMETSAT and TNO/Selex Galileo.

1.2 Document Structure

The document is separated into two main chapters. Chapter 2 describes investigations and changes applied to the on-board definition of PMD band settings, which triggered an investigation and update of the spectral calibration of PMD data. Chapter 3 is dedicated to changes that affect the quality of the PMD signal calibration and consequently the quality of the derived Stokes fractions, which are used directly by scientific users but are also applied for polarisation-correcting the main channel radiances of the instrument.

1.2.1 Chapter 2

Chapter 2 is subdivided in the description of the origin and adaptation PMD band definitions from version 1.0 (Chapter 2) to version 3.0 (Sections 2.2 to 2.5) and the parallel upgrade of the Product Processing Facility (up to PPF 3.9; changes to PPF 3.9 apply also to later versions of the PPF) improving both the spectral calibration of PMDs and the performance of the band definitions in view of correction of the FPA data (Sections 2.6 and 2.7).

The previously updated version of band definitions (v2.0) has been uploaded for testing purposes for one day during 8-9 October 2007 (see Section 2.3). However, in-house investigations in collaboration with the SRON polarisation study group have revealed more fundamental problems with the PMD spectral calibration key-data for FM3 (EUM.EPS.AR.9064) (Section 2.4), which finally led to a third revision of the PMD band definitions tagged v3.0 (Section 2.5).

In Section 2.5 the document evaluates the impact of the new PMD band definitions v3.0 on the key parameters derived from PMD data employing PPF version 3.8 with GOME INS auxiliary file version 1.19 which are used to characterise the polarisation dependence of the main channels.

Sections 2.6 and 2.7 describe the impact of all changes applied on the offline processed level 1B data quality and the results from a second one-day test campaign carried out on 6-7 February 2008.

The structure of Chapter 2 of this document follows the history of findings and improvements which led to the current final status on PMD band definitions v3.1 and PMD spectral calibration as applied to the level 0 to 1B processor 3.9.

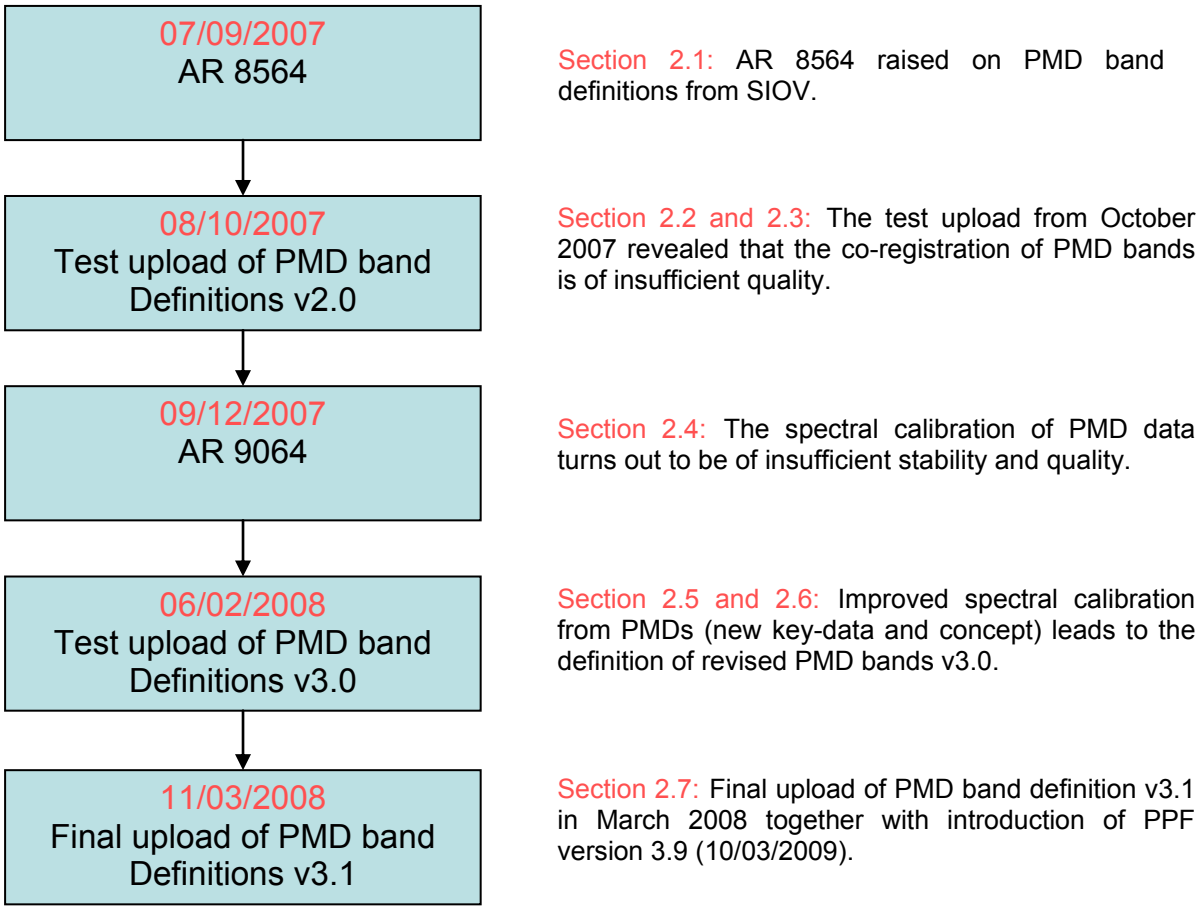

Schematic of the processor and band-definition improvement as documented here.

1.2.2 Chapter 3

During the course of the investigations on spectral calibration of PMD and band definitions, additional issues predominantly concerning the viewing angle dependence of the PMD calibration have been addressed and the findings leading to the introduction of a new online correction scheme for Stokes fractions are summarised in Chapter 3.

Chapter 3 of the document describes the update on PMD signal calibrations as implemented for PPF version 4.3 and 4.4 and later versions.

1.2.3 Appendices

Appendix A provides evaluation results based on off-line processing of level 0 data from the 8-9 October 2007 test upload and from reference data orbits taken shortly afterwards. The processor version used at this time was 3.7.0 in conjunction with the GOME-2 auxiliary initialisation file 1.17.

Appendix B details the close relationship between long-term variations in spectral calibration of PMDs and (differential temperature) long-term dependencies of the individual PMD detectors.

Appendix C finally summarises all changes introduced to the processing of Stokes fractions for level 1 data (PPF 3.9 to 4.2) before the introduction of the new online correction scheme with processor version 4.3.

All level 1B data displayed here have been processed in the EUMETSAT Technical Computing Environment (TCE).

1.3 Open Issues and Assumptions

The on-board PMD band definitions are defined with respect to detector pixel number. The given and actual centre wavelength and wavelength range covered per PMD band therefore depend on the actual spectral calibration of the PMD channels and its stability (see also General Limitations section 1.5).

1.4 Documents

1.4.1 Applicable Documents

AD0	GOME-2 L1 Product Generation Specification	EPS.SYS.SPE.990011
AD1	GOME-2 Instrument Operations Manual	MO-MA-ESA-GO-0304
AD2	GOME-2 L1 Product Format Specification	EPS.MIS.SPE.97232
AD3	GOME 2 FM3 calibration: Polarisation response	MO-TR-TPD-GO-0099
AD4	GOME-2 L1B Product Validation Report No. 3: Operational Status	EUM.MET.REP.08.0103

1.4.2 Reference Documents

RD0	GOME-2 Design Specification Science Data Packet (Format) Definition (SDPD)	TL15033-MO-DS-LAB-GO-0008
RD1	GOME-2 Polarisation Study – Final Report	SRON-EOS-RP-08-033

RD3	GOME-2 FM3 Long-Term In-Orbit Degradation - Analysis, Test Results and Mitigating Action Plan	EUM/OPS-EPS/TEN/08/0588
RD4	GOME-2 FM3 key-data update	MO-TN-TPD-GO-0085
RD5	GOME2 calibration specialist meeting, MOM - TNO, Delft 2009	MO-MN-TPD-GO-0163
RD6	Investigations on polarisation issues	MO-MN-TPD-GO-0083
RD7	GOME2 calibration specialist meeting 3rd September 2009	MO-MN-TPD-GO-0164

1.5 General Limitations

The implemented changes of PMD band definitions are based on PMD pixel position and therefore based on the overall accuracy of the spectral calibration for PMD P and S at the time of whatever reference orbit was used.

2 PMD BAND DEFINITION AND PMD SPECTRAL CALIBRATION

2.1 Default PMD Band Definitions from SIOV Campaign (used until 11 March 2008)

The default on-board PMD band definitions v1.0 [AD1, Table 1] have been used during on-ground calibration of the instrument. ESA-SSST has therefore decided to use the same definitions during the instrument In-Orbit Verification (IOV) phase.

Band	First pixel in band from C-start	Number of pixels in Band	Start Wavelength λ(nm)	Stop Wavelength λ (nm)
0	19	2	309.2	309.9
1	23	5	311.7	314.4
2	31	4	317.0	319.1
3	37	12	321.2	329.5
4	50	5	331.1	334.3
5	56	43	335.9	377.7
6	100	4	380.1	383.7
7	115	20	399.3	428.4
8	138	43	435.5	552.5
9	183	2	553.6	557.5
10	187	22	569.6	678.6
11	217	2	742.3	750.2
12	219	1	758.2	758.2
13	223	1	792.1	792.1
14	228	1	838.8	838.8

Table 1: Default GOME-2 PMD band definitions (v1.0), from the GOME-2 IOM, page 125 [AD1]

Note that only one set of values exists as default for both PMD channels [AD2] assuming spectral co-registration of the PMD.

The definitions thereafter remained uploaded on board after IOV until completion of the study on PMD calibrations and new PMD definitions (suggested by GSAG) at 11 March 2008. The result of this study is documented in the following chapters.

2.2 PMD Band Definitions as Suggested by GSAG

In 2004, the GOME Scientific Advisory Group (GSAG) endorsed a list of PMD parameters as suggested by the Netherlands Institute for Space Research, SRON, and adapted to PMD detector pixel number by Joerg Callies from ESA/SSST. Table 2 lists the original suggestion by Otto Hasekamp from SRON (blue columns) as endorsed by GSAG, and the adapted ones for the GOME-2 instrument based on on-ground calibration measurements for PMD-S and P (green and red respectively).

	input based on SRON Otto Hasekamp				GOME203 PMD -S					GOME203 PMD-P				
band	wavelength 1	wavelength 2	width	FWHM	wl 1	wl 2	px 1	px 2	width	wl 1	wl 2	px 1	px 2	width
0	311.8	314.3	5	3.1	311.75	314.3	787	792	6	311.94	314.5	786	791	6
1	316.9	318.8	4	3.3	316.89	318.47	797	800	4	317.09	318.68	796	799	4
2	321.5	329.3	12	3.5	321.21	329.2	805	818	14	321.44	329.49	804	817	14
3	330.8	334.6	6	3.8	331.27	334.92	821	826	6	330.87	334.49	819	824	6
4	336.2	340		4.2	335.69	339.67	827	832	6	336.01	340.02	826	831	6
5	361	377.9	17	4.8	360.71	377.1	854	868	15	361.1	377.49	853	867	15
6	380.3	383.9	4	6.1	379.64	383.53	870	873	4	380.02	383.92	869	872	4
7	399.8	428.9	19	7.8	398.8	429.39	884	903	20	399.18	429.77	883	902	20
8	435.1	493.5	23	10.2	436.66	494.72	907	933	27	435.21	492.57	905	931	27
9	495.5	552.4	23	12.5	494.72	552.04	933	951	19	495.26	552.79	932	950	19
10	552.4	556.2	2	18.7	552.04	555.69	951	952	2	552.79	556.59	950	951	2
11	567.9	614	11	25.3	567.65	612.65	955	965	11	568.45	613.61	954	964	11
12	619	660	5	25.3	622.82	661.98	967	974	8	618.65	657.1	965	972	8
13	743.1	766.6	3	38.5	744.32	768.82	986	989	4	745.57	769.72	985	988	4
14	783.6	792.4	2	43.9	785.38	794.14	991	992	2	786.69	795.45	990	991	2

Table 2: GOME-2 PMD band definitions as endorsed by GSAG (blue columns) and as adapted by ESA/SSST (green and red columns)

2.3 PMD Band Definitions v2.0 as Adapted by EUMETSAT for Test Upload on 8-9 October 2007

The PMD spectral calibration has changed significantly for PMD-S with respect to on-ground measurements. Therefore, the PMD-S band-definition pixel numbers in particular had to be revised with respect to the numbers provided by ESA/SSST, in order for P and S to cover approximately the same wavelength regions. In addition, the separation pixel between Block C and D of the PMD data readout (different integration times) has to be shifted, since the on-board processor does not allow one band to extent over this border. For the latter change the length of Block B has been shortened from 23 to 18 detector pixels [AD0, Appendix B] for both PMD S and P. The evaluation of PMD band definitions v2.0 has been based on the level 1B spectral calibration of PMD data from processor version 3.7.0 for orbit 3372 on 14 June 2007 (see Table 3).

Note: this revised band definition set version 2.0 has been derived on the basis of the original key-data set. As has already been observed before the time of the first test upload of the revised set on 8-9 October, the processing of the spectral calibration coefficients in the GOME-2 operational level 0 to 1B processor (PPF) has been quite unstable, i.e. unstable convergence of the FPA to PMD cross-correlation coefficients optimisation scheme (for details of the processing of PMD spectral calibration we refer to [AD0]). As described in the following chapter the root cause of this instability has been found to be the insufficient accuracy of the polynomial representation of the spectral dispersion of PMD data. As a consequence, version 2.0 of the PMD band definitions has not been uploaded again, because the resolution of this problem induced a new band definition set (v3.0; see Section 2.5).

Band-S No.	pix1	pixw.	wav1	wav2	Band-P No.	pix1	pixw.	wav1	wav2
0	22	5	311.5919	314.0893	0	18	5	312.0035	314.3942
1	30	4	316.6438	318.5998	1	26	4	316.8348	318.7035
2	37	12	321.2659	328.991	2	33	13	321.2537	329.3938
3	50	6	330.466	334.2612	3	47	6	330.8337	334.5525
4	57	6	335.825	339.8575	4	54	6	336.0903	340.0692

5	85	16	361.0732	377.7722	5	82	16	361.1994	377.9004
6	102	4	380.1987	383.9339	6	99	4	380.3255	384.0568
7	117	19	400.1117	428.7835	7	114	19	400.1888	428.6639
8	138	27	434.1853	491.5447	8	136	27	435.8433	493.3494
9	165	18	494.231	547.7581	9	163	18	496.0442	549.785
10	183	2	551.4519	555.2166	10	181	2	553.4959	557.2784
11	187	11	566.956	611.534	11	185	11	569.074	613.8691
12	198	9	616.5106	660.3022	12	196	9	618.8693	662.8536
13	218	4	741.7938	765.7213	13	216	4	744.5909	768.5558
14	223	2	782.5728	791.2811	14	221	2	785.4234	794.1367

Table 3: GOME-2 PMD band definitions (v2.0) as adapted by EUMETSAT based on level 1B spectral calibration of PMD data from PPF version 3.7.0 from orbit 3372 (14 June 2007) taking into account the changes in spectral calibration and Block C/D transition. This set of definitions has only been uploaded for orbit 5024 to 5038 during 8-9 October 2007.

Figure 1 shows the new PMD band positions v2.0 (lower panel) with respect to the old ones v1.0 (upper panel) and the improved overlap between PMD-P and S band positions especially in the IR region.

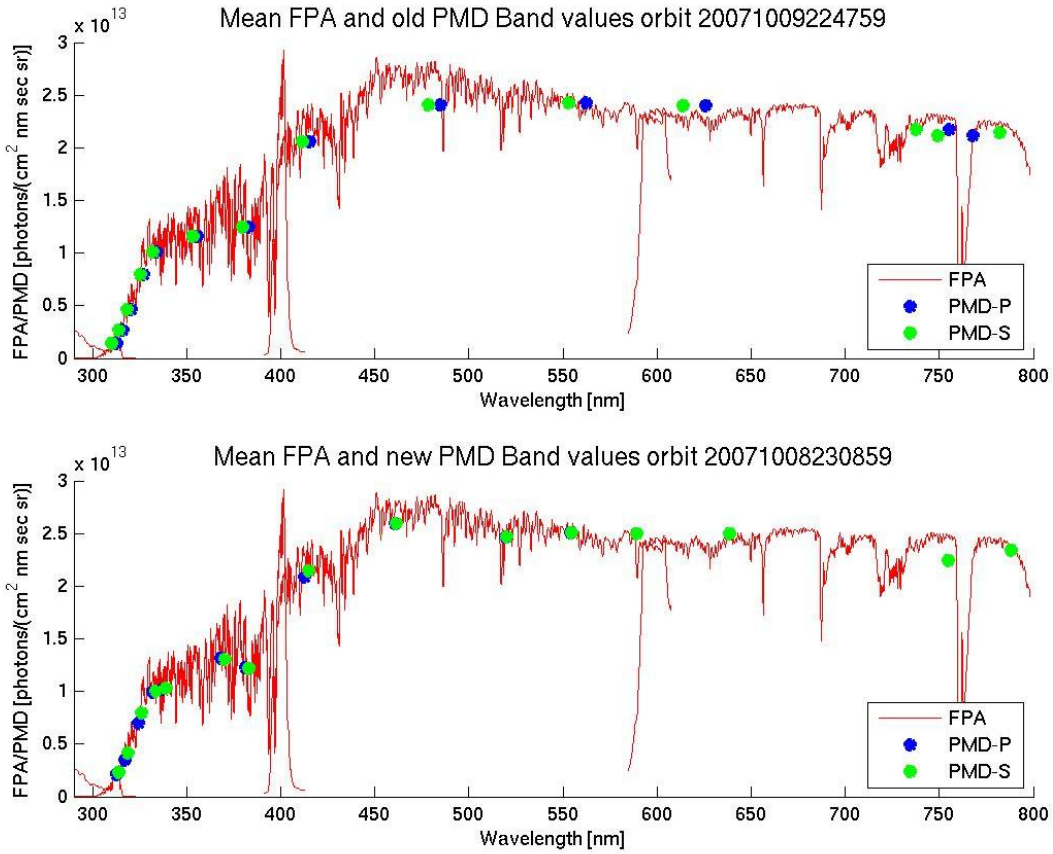

Figure 1: Comparison between PMD band radiances based on previous PMD band definitions (upper panel), and as used during SIOV and new GOME-2 PMD band radiances based on the new definitions (v2.0) as endorsed by GSAG (lower panel)

Starting with processor version 3.7.0 and in order to account for any remaining differential shift in wavelength between P and S (e.g. because of long-term changes in spectral stability and/or sub-detector pixel relative shifts), an interpolation of PMD-p and PMD-s PMD data, onto a common spectral grid, has been introduced. After applying the interpolated ratios during processing, the final results in PMD radiances are interpolated back onto the actual spectral grid for P and S. The result of the latter can be seen from the lower panel where the blue and green dots, even though shifted in wavelength, follow better the FPA spectral dependence as expected.

A detailed discussion of the impact of the upload of the PMD band definitions v2.0 during 8-9 October on key parameters of the level 1B data is provided in Appendix A.

2.4 Key-Data Problem Affecting the Processing of PMD Spectral Calibration Coefficients (EUM.EPS.AR.9064, December 2007)

2.4.1 Introduction and Summary

During the first year of operations of the GOME-2 instrument the spectral calibration of PMD data, on which the analysis of improved band definitions is based, has always been a matter of concern (see figures provided in Appendix B),

1. because there appears to be a difference between the long-term changes of both PMD P and S, and
2. because the in-flight spectral calibration shift for PMDs as employed by the level 0 to 1B processor appeared to be somewhat unstable.

The first issue is currently still under investigation and may well be related to a differential long-term through-put degradation of both PMD S and P signals (cf. Figure 21 in Chapter 3).

The second issue appears to be closely linked to a problem in the underlying key-data representation of the PMD spectral grid together with its polynomial representation of the dispersion, which appears to be an inadequate representation of the real dispersion. The errors introduced by the latter also appear to be much stronger for FM3 than for FM2 (not shown here).

The purpose of the following analysis based on key-data only (i.e. based on on-ground key-data reference measurements) is to demonstrate that:

1. the differences in spectral dispersion between convolved measurements from the instruments spectral light source using the FPA and PMD on-ground measurements from an independent monochromator (see key-data documentation) are quite large for some spectral windows;
2. the slit function measurements are especially sparse in the most problematic spectral regions and that, as has been done for FM2, the PMD slit function needs to be provided at many more spectral points along the PMD dispersion;

3. the distribution of the initial spectral differences (delta shifts) between FPA convoluted and direct PMD measurement points along the spectral axis point to a problem in the polynomial representation of the underlying "real" spectral dispersion of PMDs for FM3.

As a consequence of the results of the analysis we suggest the following concerning instrument key-data for PMD (EUM.EPS.AR.9064):

1. Provide a re-measured initial calibration of the PMD detectors based on better characterisation of the PMD slit functions and using SLS FPA data for calibration.
2. Do not use a polynomial representation of the spectral dispersion for PMD FM3 neither for key-data nor during level 0 to 1B processing, or, alternatively, re-evaluate the on-ground data and derive a more accurate representation.

As a short-term or intermediate solution for level 0 to 1B processing addressing most of the current issues on PMD data quality (EUM.EPS.AR.9064, EUM.EPS.AR.9103) we suggest:

1. An initial correction of the PMD key-data spectral grid employing a p-spline fit to delta shifts between key-data FPA-SLS measurements and key-data PMD-SLS measurements. The resulting shifted grid should then be used as an initial guess for PMD wavelength calibrations throughout the processing.
2. Employ a linear fit to on-board SLS measurements and their delta-shifts as has been done before, but using the revised initial PMD grid.
3. Do not use any polynomial representation of PMD spectral dispersion throughout the processing (including key-data).

Note that point 3 of the above will make an update of the PFS 7.1 necessary, however affecting level 1A output only (i.e., replacing PMD wavelength coefficients in VIADR-1a-spec with the full spectral grids for PMD-P and S).

2.4.2 Analysis of Closed Loop PMD Spectral Calibration Using Key-Data Measurements

2.4.2.1 Inputs

The inputs to the following analysis of a closed-loop spectral calibration of PMDs using FPA on-ground SLS measurements are key-data measurements (FM3, 203) of SLS data provided in BU/s for both FPA and PMDs. The files used are:

SLS for FPA:	WL_SLS_MAIN.203 (version 1.2)
SLS for PMD:	WL_PMD_P.203 (version 1.2); WL_PMD_S.203 (version 1.2)
Spectral calibration for FPA:	WL_MAIN.203 (version 1.2)
Slit functions for PMD:	WL_SLIT_PMD_P.203 (version 1.2); WL_SLIT_PMD_P.203 (version 1.2)

The equidistant grid is defined as for the in-flight PPF processing (see [AD0]) using 65536 spectral points between 289.568 and 999 nm (cf. INS auxiliary file for GOME-2 version 1.17ff).

2.4.2.2 Convolution (PGS 6.1; 5.2.16.4 step 1 to 14)

The convolution is carried out offline using a MATLAB code following the individual steps as laid out in the PGS 6.1 [AD0, Section 5.2.16.4], except for steps 3 to 7 dealing with the calibration of the FPA-SLS measurements employing MMEs (Eq. 164). We avoid the calibration using MMEs until their consistent update with respect to PMD spectral calibration (since the latter is supposed to also affect PMD MME data). The convolved SLS spectrum from the FPAs will be slightly affected by this issue providing different weights to different line strengths per cross-correlation window. However, this does not affect the relative line-positions, i.e. we consider the effect on the results of the cross-correlation algorithm to be small. Similar considerations hold for the preparation of PMD data employing MMEs (Eq. 167) in step 13 and 14. For the offline cross-correlation between convolved FPA-SLS data and PMD-SLS data Eq. 167 is not applied.

Figure 2 to Figure 8 provide the results of the convolution, the original SLS FPA key-data spectrum and the PMD reference spectrum (also from key-data) for all seven cross-correlation windows newly defined for the offline calculations. The start/stop wavelengths of these windows are summarised in the following table:

Windows	1	2	3	4	5	6	7
Start [nm]	295.06	325.0	348.4	382.4	403.0	486.9	583.5
Stop [nm]	315.64	345.0	381.0	401.0	471.0	554.0	718.0

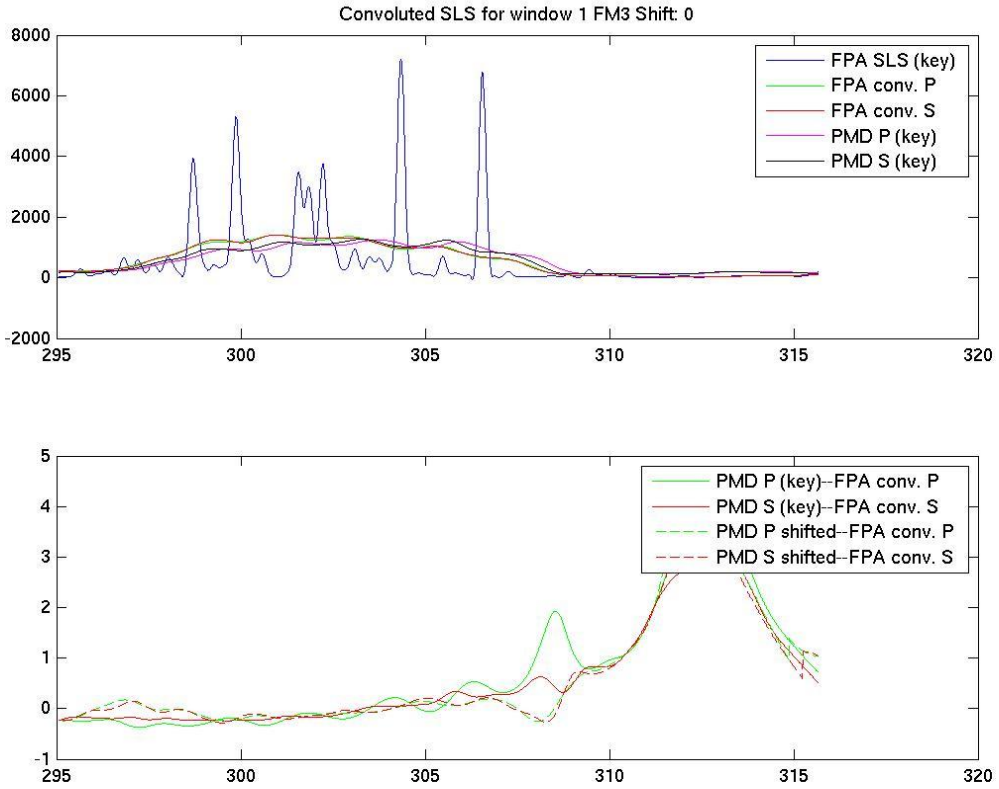

Figure 2: 1st cross-correlation window. Upper panel: Original FPA SLS measurement from key-data (on-ground) in comparison to the offline convolved FPA SLS and on-ground PMD SLS measurements for both PMDs. Lower panel: Difference between convolved FPA SLS and PMD SLS before cross-correlation (solid lines) and after cross-correlation shifting of PMD wavelength grid (dashed lines).

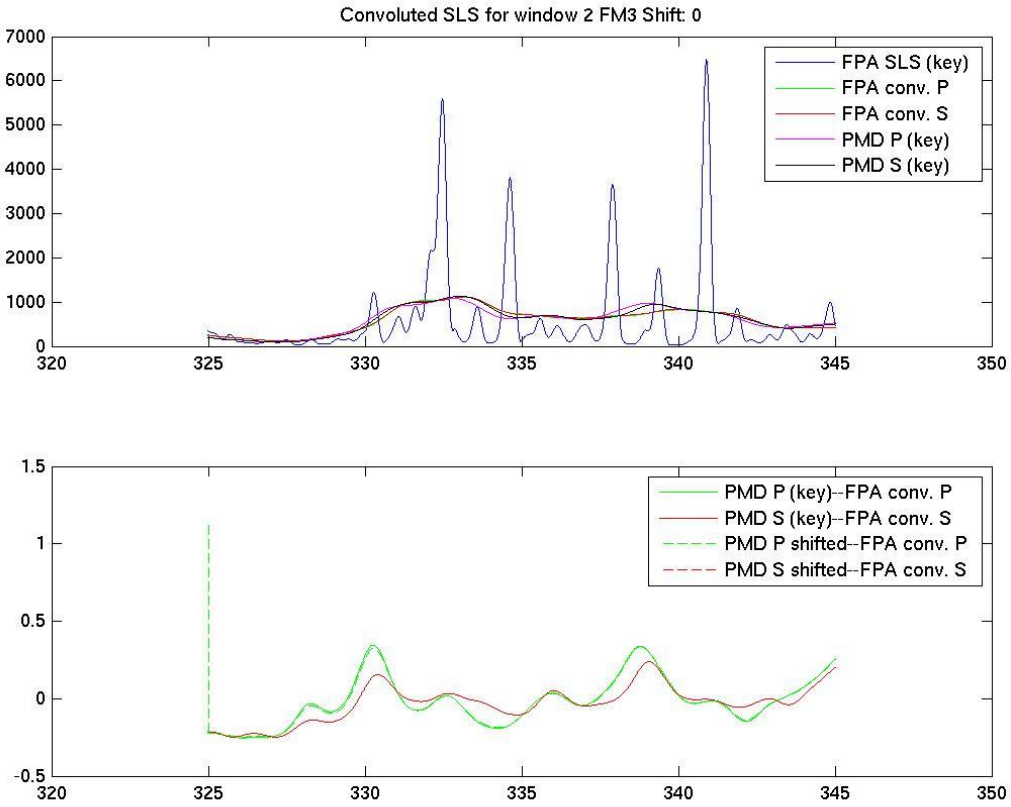

Figure 3: 2nd cross-correlation window

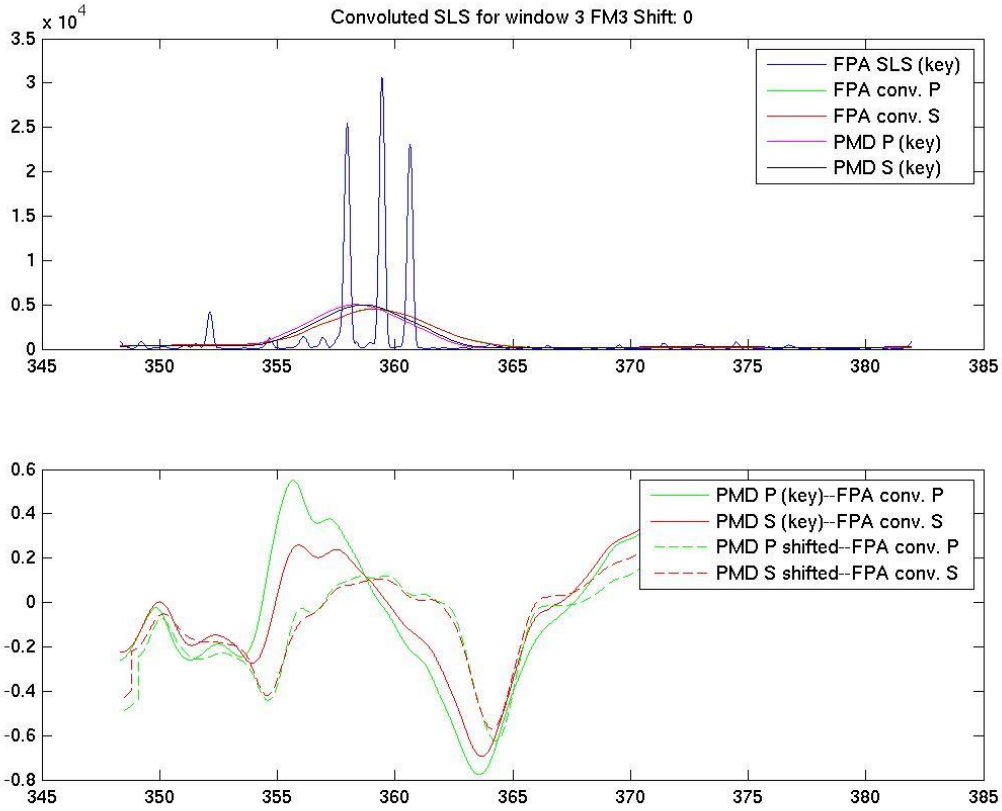

Figure 4: 3rd cross-correlation window

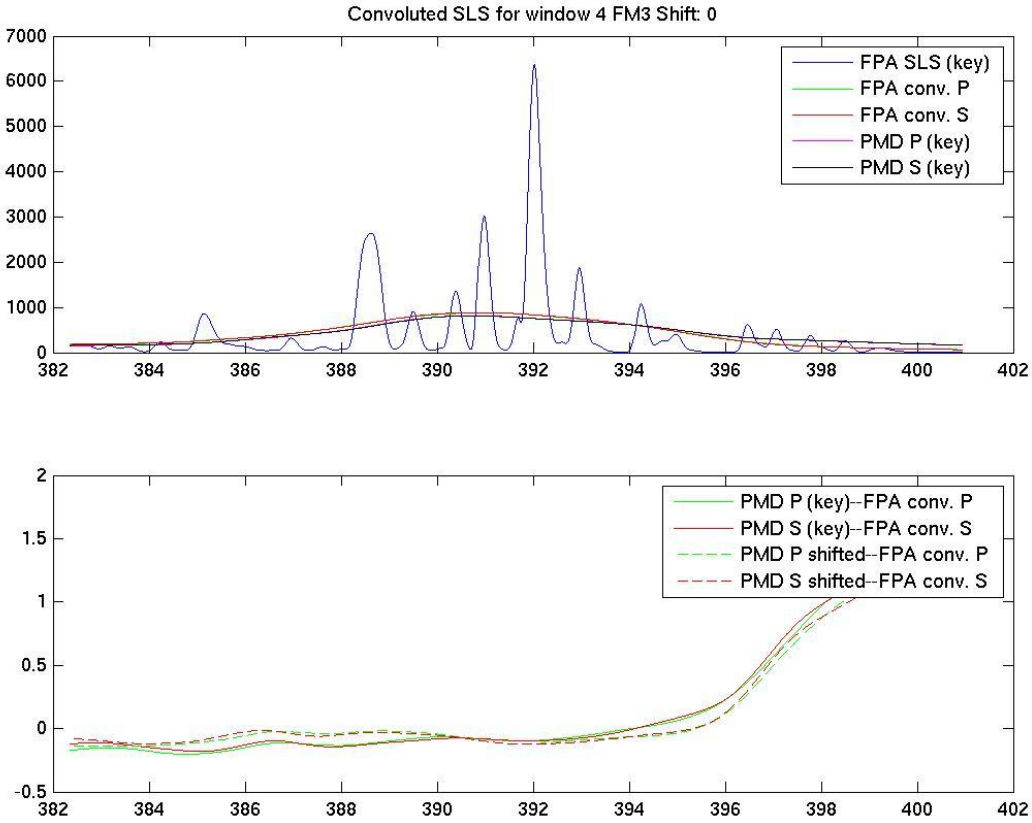

Figure 5: 4th cross-correlation window

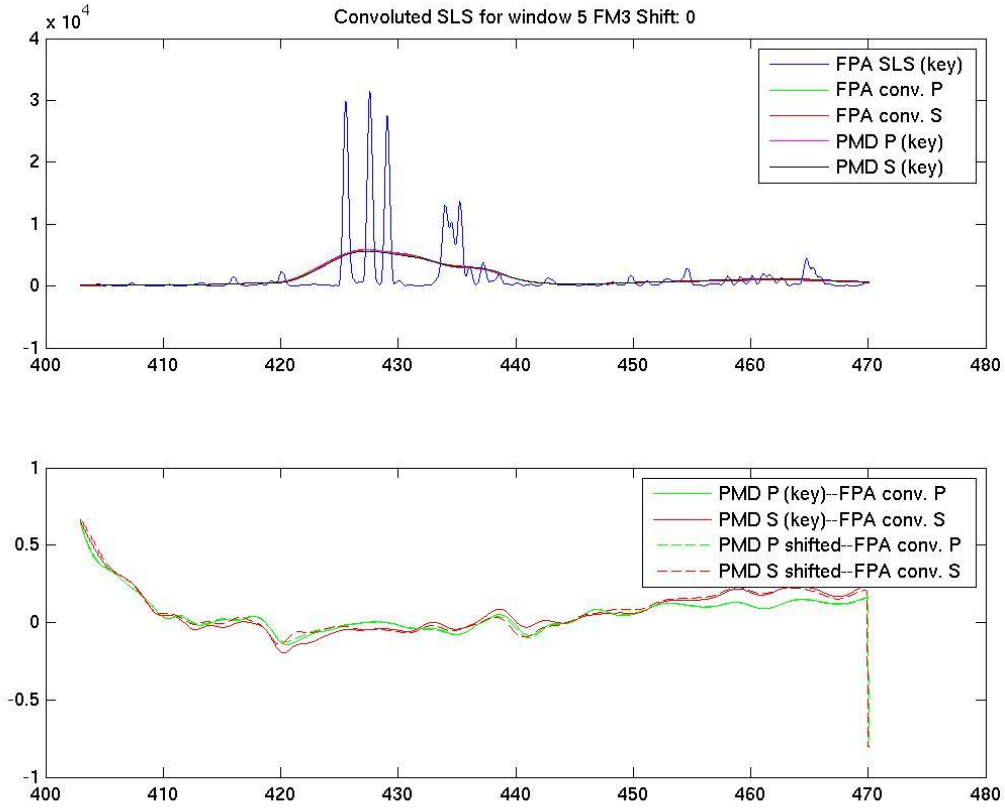

Figure 6: 5th cross-correlation window

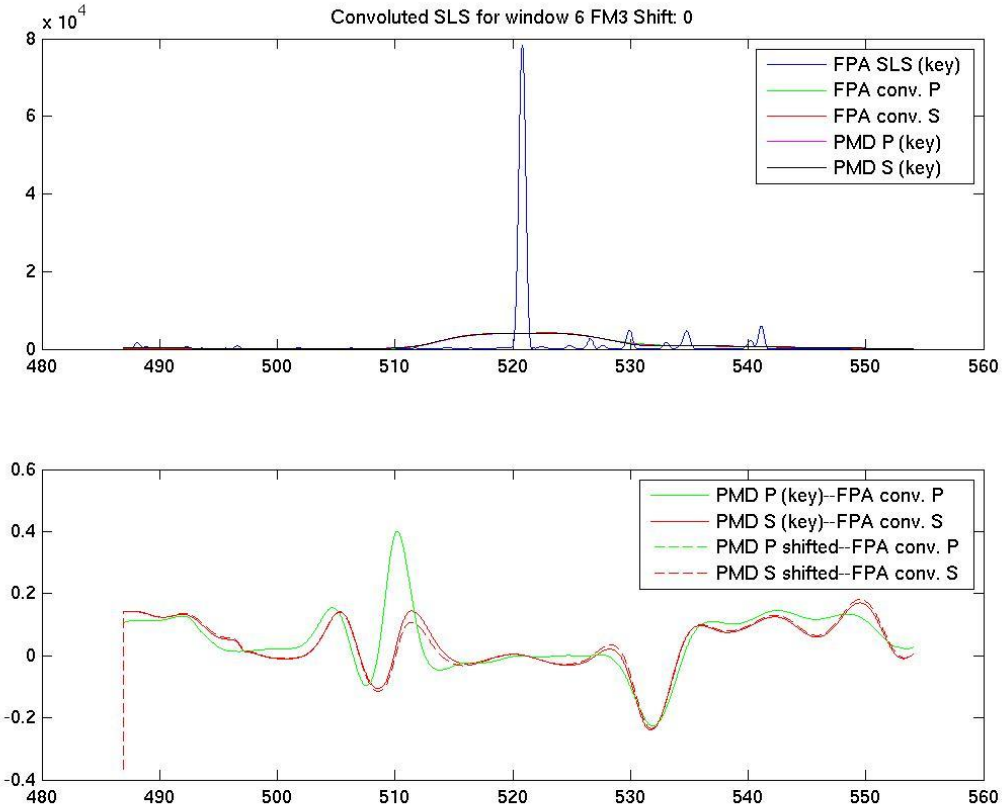

Figure 7: 6th cross-correlation window

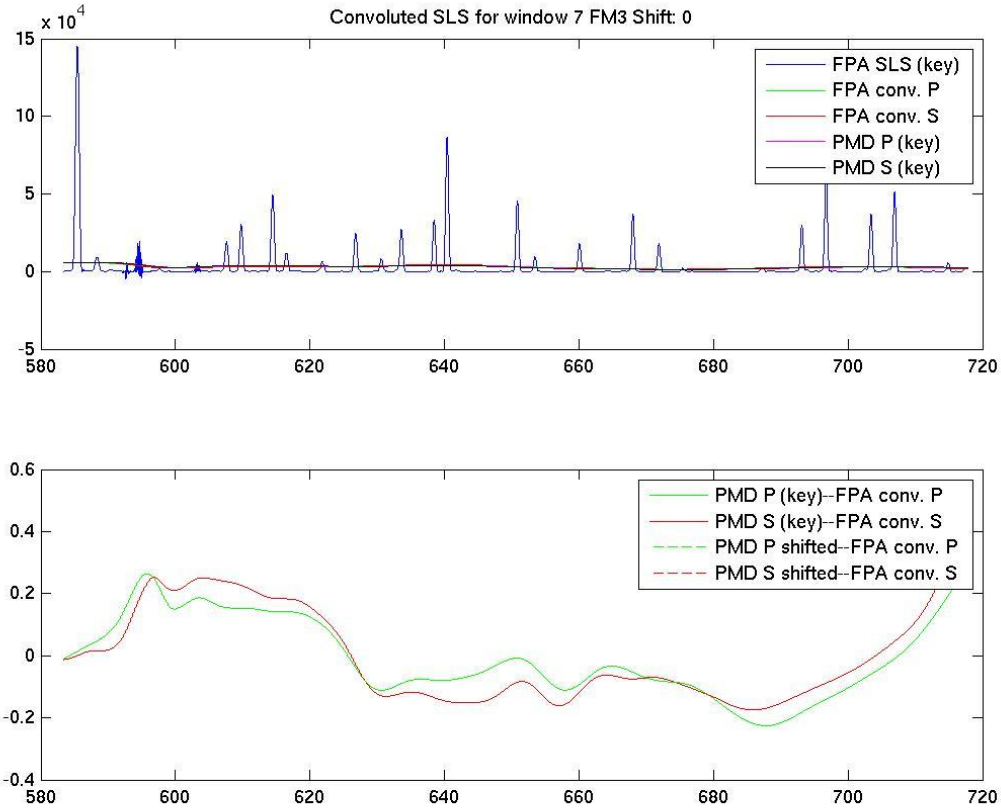

Figure 8: 7th cross-correlation window

2.4.2.3 Cross-Correlation (PGS 6.1; 5.2.16.4 step 15 to 19)

The cross-correlation as laid out in PGS 6.1; 5.2.16.4 steps 15 to 19 is carried out using the cross-correlation function of MATLAB "xcorr" (the PPF cross-correlation has been streamlined to produce the same results). For each window the accumulated wavelength shifts between the convolved FPA-SLS and PMD-SLS spectra needed in order to achieve an optimal correlation are plotted in Figure 9 (stars). The accumulation occurs during an iterative process terminated when the remaining shift is smaller than 0.02 nm on the equidistant grid.

Note, there appears to be a gap in the key-data representation of the PMD slit function exactly around the largest shifts (~380 nm) for FM3 (see Figure 9) which, in contrast, is represented for FM2 by explicit slit function measurements.

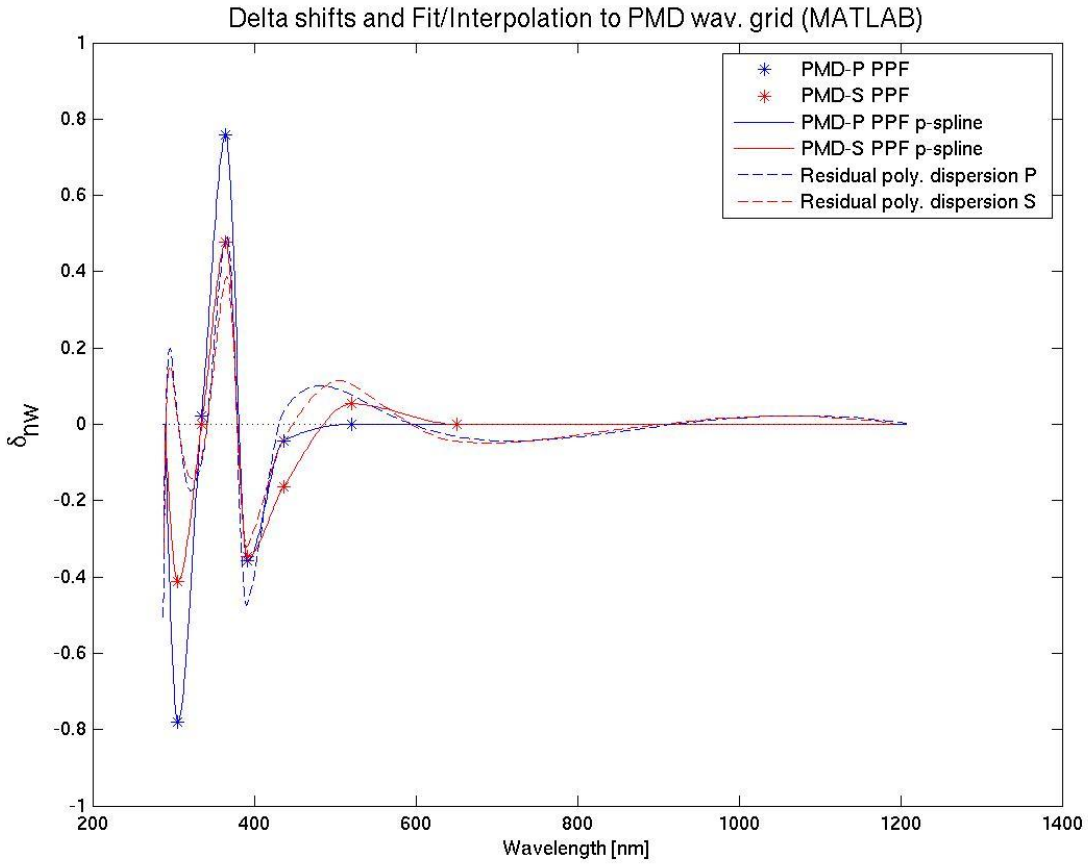

Figure 9: Delta shifts per window evaluated after cross-correlation (stars) for both PMD grids and with respect to the original PMD wavelength grid in the key-data. The solid lines denote a piece-wise spline through the shifts. For comparison the residual between the original grid and a polynomial representation of 6th order of the PMD grid is given in dashed lines.

2.4.2.4 Representation of Shifts on Full Equidistant Grid (PGS 6.1; 5.2.16.4 step 20)

The PGS specifies a linear fit to be applied through each of the seven delta shifts carried out on the equidistant high resolution grid. The solution of this fit can then be subsequently applied to shift the full grid. From a visual inspection of the results in Figure 9 one can however already see that a linear fit would not provide an appropriate solution for the underlying distortion of the initial PMD wavelength grid (as measured on-ground). A piece-wise spline-fit as shown in Figure 9 (solid line) provides a much better representation of the overall shifts and already suggests a polynomial type of distortion to the underlying spectral dispersion.

2.4.2.5 Representation of (Shifted) Wavelength Grid Employing a Polynomial (PGS 6.1; 5.2.16.4 step 21)

Figure 10 shows various representations of the PMD wavelength grid, shifted or not (!), by various orders of polynomials as specified in PGS 6.1; 5.2.16.4 step 21. The plot displays the difference between the original grid and its polynomial representations both in a relative and an absolute sense. In addition Figure 9 of the previous section also shows the error of a polynomial representation of 6th order (as currently employed in the PPF) as dashed lines. We conclude that a 6th order error of the polynomial representation very closely resembles the observed distortion between the initial key-data grid and the convolved FPA-SLS cross-correlated measurements. This points to a systematic problem in representing the real PMD spectral dispersion for FM3 with any (!) type of polynomial (see also residuals of higher order polynomials in Figure 10).

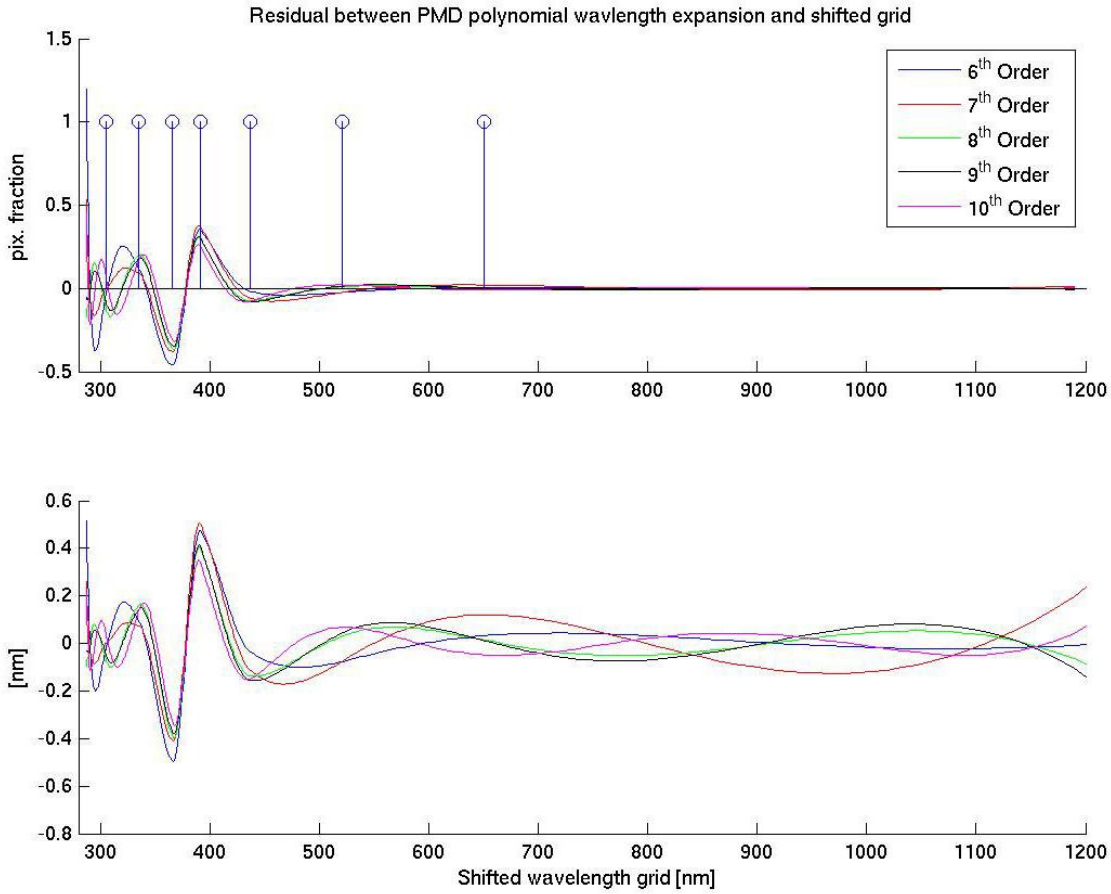

Figure 10: Residual between the full initial PMD wavelength grid and its polynomial representations using various degrees of polynomials. The differences are given in pixel fraction (upper panel) and wavelength (lower panel). The vertical lines denote the centre position of the cross-correlation windows.

2.4.2.6 Impact on the Stability of the Spectral Calibration of the PMD Algorithm Employed for all PPFs up to Version 3.7.0

Figure 11 shows repeated cross-correlations between the convolved FPA-SLS with PMD-SLS data for which after each cross-correlation the wavelength grid for both PMDs has been shifted according to the derived delta shifts. The left panels (higher panel PMD-P; lower Panel PMD S) show results employing the original strategy, where each shifted PMD wavelength grid has been transferred into a polynomial representation first before using again with the next cross-correlation. The right panels shows the same but then without transformation into a polynomial in-between, i.e. always using the fully shifted grid. The results show that the procedure converges at a sub-pixel level for the latter strategy, whereas the error on the polynomial representation is always reintroduced for the first procedure.

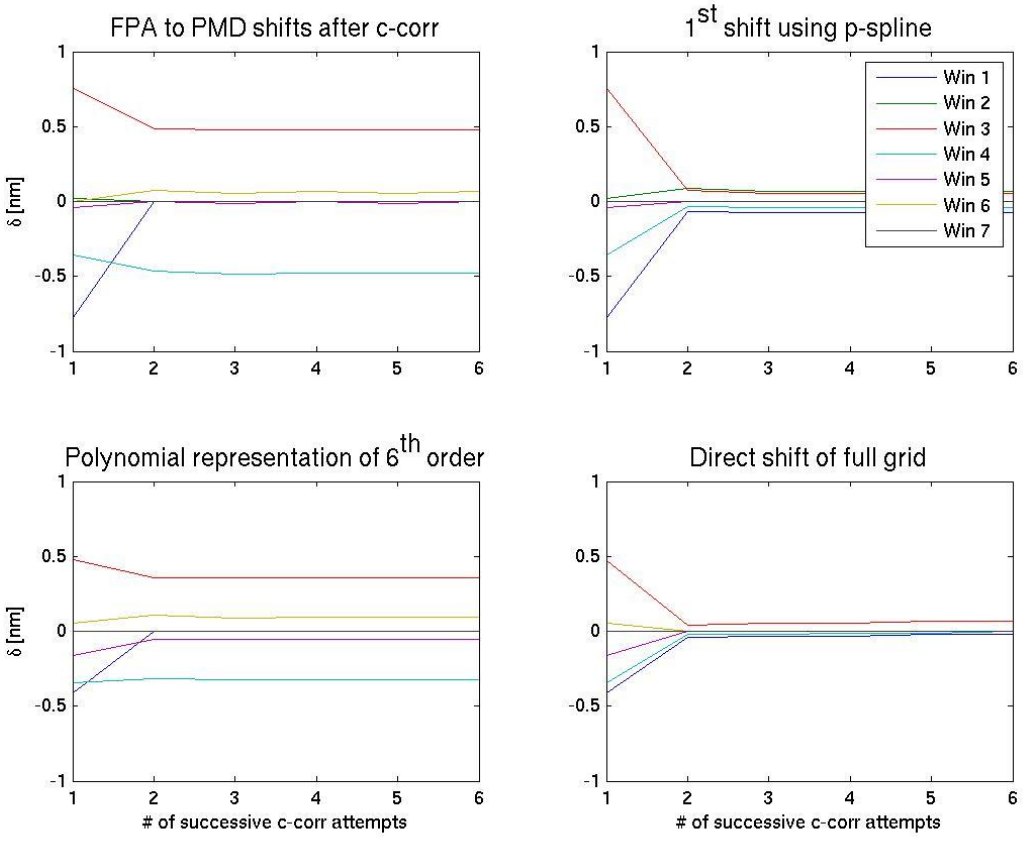

Figure 11: The panels show delta-shifts of successive cross-correlations carried out starting with the shifted grid of the previous cross-correlation result. The left column shows results for P and S (upper and lower panel) for which, after each cross-correlation, the shifted grid is represented by a 6th order polynomial as specified in PGS 6.1. The right column shows the same but always employing the full spectral grid. The first evaluation of the individual shifts on the equidistant grid is done using a p-spline function. All subsequent delta results are represented on the equidistant fine-grid using a linear fit as specified in the PGS 6.1.

2.4.2.7 Impact on Key-Data for PMDs

As a consequence of the previous results, all PMD calibration-related key-data files providing or using a representation of the spectral grid during processing of raw data require an update. The most important of these are α, β, γ and ζ (see e.g. [AD0] for characterisation of Mueller Matrix Elements MMEs) characterising the radiative and relative polarisation response of the PMDs and the direct (ir)radiative response functions. For processing of raw calibration data the polynomial representation of the on-ground measured PMD spectral grid has been used (see [AD3], 5.2.3), which has been violated by the previous findings.

During a meeting at Galileo Avionica, Florence, with TNO, the Netherlands, responsible for GOME-2 Flight Model characterisation, it has been agreed that these issues have to be taken into account in a consistent reworking of the key-data set (including improved slit function characterisation) used as input for the delta-calibration campaign (see [RD5]). Until this kind of consistent reanalysed data set becomes available we have used calibration raw data for FM3 and the original IDL source-code used for key-data production and consistently replaced the polynomial representation of the spectral grid by the full grid, as laid out in the previous sections and for those key-data files used in the current processing. From this we derived the following updated set of key-data files:

POL_ALPHA.203
POL_BETA.203
POL_GAMMA.203
POL_ZETA_PMD_P.203
POL_ZETA_PMD_S.203
RA_ABS_RAD_PMD_P.203
RA_ABS_RAD_PMD_S.203
RA_ABS_IRR_PMD_P.203
RA_ABS_IRR_PMD_S.203

The modifications have led to new versions of the above files (indicated in the header of the files: all files are tagged as version 1.3 and a reference to this document has been added!) which in turn have been added to a new release by EUMETSAT of the calibration-data auxiliary file (GOME_CAL_M02_*) tagged 1.03/FM3x391.

Note that ultimately all key-data grids for PMDs should be updated consistently, also those not used for the current level 0 to 1B processing!

The full spectral grid of on-ground key-data measurements used as an initial grid for spectral calibration during level 0 to 1 processing ([AD0], 5.2.16) has been added in two key-data files

WL_PMD_P_GRID.203 and
WL_PMD_S_GRID.203,

which are used throughout the processing starting with processor version 3.8.0 (installed in the GS since 29 January 2008) plus higher versions. Results discussing the impact on the PMD calibration following these changes are shown in Section 2.6.

2.5 Revised PMD Band Definitions v3 Following Key-Data Upgrade

Following the empirical correction of key-data for PMD spectral calibration as laid out and discussed in the previous chapter, we evaluate the impact on our adaptation of the GSAG proposal for PMD band definitions (see Chapter 2, Table 2) for a reprocessed version of the previously-used reference orbit 3372 on 14 June 2007. The reprocessing has been done with PPF version 3.8 and with all necessary changes to the algorithm for improving the spectral calibrations implemented (see Section 2.4). The new PMD band definitions version 3 derived from this version of the PPF are tabulated in Table 4.

Band-S No.	pix1	pixw.	wav1	wav2	Band-P No.	pix1	pixw.	wav1	wav2
0	22	5	311.709	314.207	0	20	5	311.537	313.960
1	30	4	316.762	318.720	1	29	4	317.068	318.983
2	37	12	321.389	329.139	2	36	12	321.603	329.267
3	50	6	330.622	334.443	3	49	6	330.744	334.560
4	57	6	336.037	340.161	4	56	6	336.157	340.302
5	84	17	360.703	377.873	5	83	17	361.054	378.204
6	102	4	380.186	383.753	6	101	4	380.502	384.049
7	117	19	399.581	428.585	7	116	19	399.921	429.239
8	138	27	434.083	492.066	8	137	27	434.779	492.569
9	165	18	494.780	548.756	9	164	18	495.272	549.237
10	183	2	552.474	556.262	10	182	2	552.967	556.769
11	187	11	568.070	612.869	11	186	11	568.628	613.680
12	198	9	617.867	661.893	12	197	9	618.711	662.990
13	218	4	744.112	768.269	13	217	4	745.379	769.553
14	224	2	794.080	803.072	14	223	2	795.364	804.351

Table 4: GOME-2 PMD band definitions (v3.1) as adapted by EUMETSAT based on level 1B spectral calibration of PMD data from PPF version 3.8 from orbit 3372 (14 June 2007). This set of definitions has been uploaded for orbit on 11 March 2008.

The new set of definitions based on in-flight data (spectral calibrations of PMD) also greatly improves the co-registration of PMD-P and S (see Figure 12). In contrast to the previous situation (v2) the co-registration shift is basically 1 for all bands except the first one. This pattern resembles exactly what has been measured on-ground.

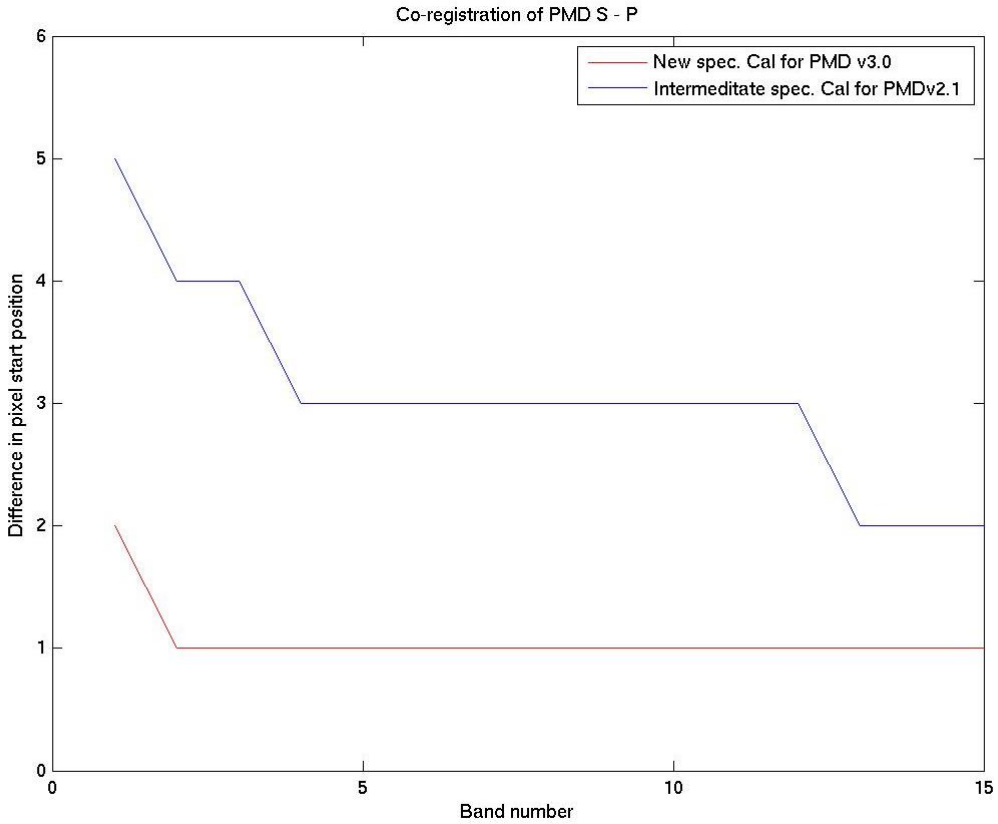

Figure 12: Co-registration of PMD band definitions for v2.1 (blue line) and v3.0 (red line) based on in-flight data from orbit 3372. V3.0 follows the behaviour that has been measured on-ground for FM3.

The largest differences with respect to v2 occur for PMD-P with pixel start shifts of the order of 2 and 3. This introduces only moderate wavelength differences of the order of 0.5 nm maximum in the UV and visible and 1 to 2 nm in the NIR. Level 2 algorithms based on PMD band positions should therefore experience only a moderate to small impact on a change of definition from v2 to 3, in contrast to the initial step from v1 to v2 with large changes in band positions.

Note, for the test upload of v3 on 5th and 6th of February a slightly different setting for band number 14 P and S has been used:

Band-S					Band-P				
No.	pix1	pixw.	wav1	wav2	No.	pix1	pixw.	wav1	wav2
14	223	2	785.285	794.080	14	222	2	786.571	795.364

Table 5: GOME-2 PMD band definitions (v3.0) as adapted by EUMETSAT used during test upload on 5-6 February 2008

After this test it was found that the band 14 for PMD-P with pixel start 222 crosses the border of PMD block D and E (see [AD0]), which causes problems in the processing of level 0 to 1. As a consequence both bands for P and S have been shifted by 1 pixel to the red (see Table 4).

2.6 Offline Validation of PPF 3.8 PMD Data Using a Revised Spectral Calibration Scheme

We make use of level 1B data derived from reference orbit 3372 measured on 14 June 2007. The processor version used is 3.7.0 (reprocessed data) for the old PMD spectral calibration scheme and 3.8 (reprocessed) data for the new scheme. The results compare key PMD measurement-derived parameters from the processing, such as Stokes fractions and P over S ratios for old and new PPF versions using SIOV (v1.0) band definitions (for new PMD band definition results v3.0 see following section).

Figure 13 and Figure 14 show the results for PMD-derived Stokes fractions plotted over single-scattering Stokes fraction values (Limiting Atmosphere test description see [AD4]). Green dots stem from back-viewing measurements, which cover forward viewing measurement results indicated in red. All blue dots fall outside the limiting atmosphere criterion and therefore indicate a degradation of the polarisation correction. When changing to the new PMD spectral calibration scheme, the quality of the Stokes fractions improves, especially in the IR and UV.

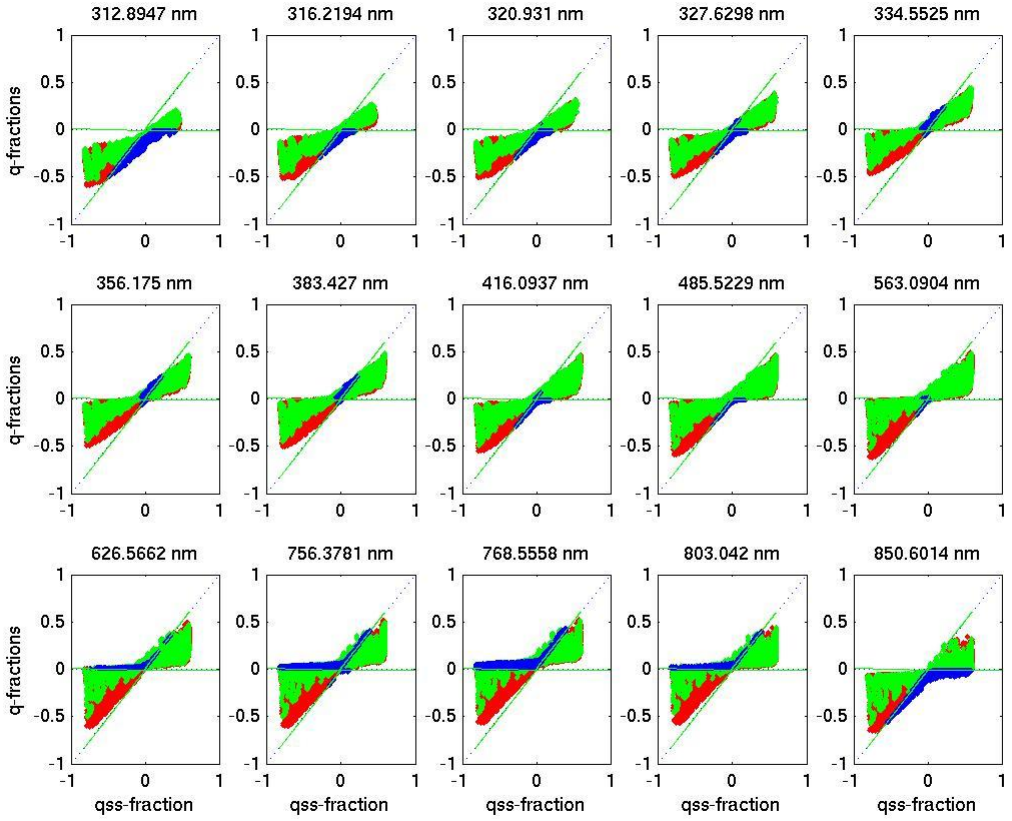

Figure 13: Limiting Atmosphere plot for all PMD bands derived Stokes fractions based on the old spectral calibration scheme used until PPF 3.7.0 and based on PMD band definitions v1.0. Green dots indicate back viewing, red forward viewing and blue dots fall outside the valid ranges defined by the limiting atmospheres.

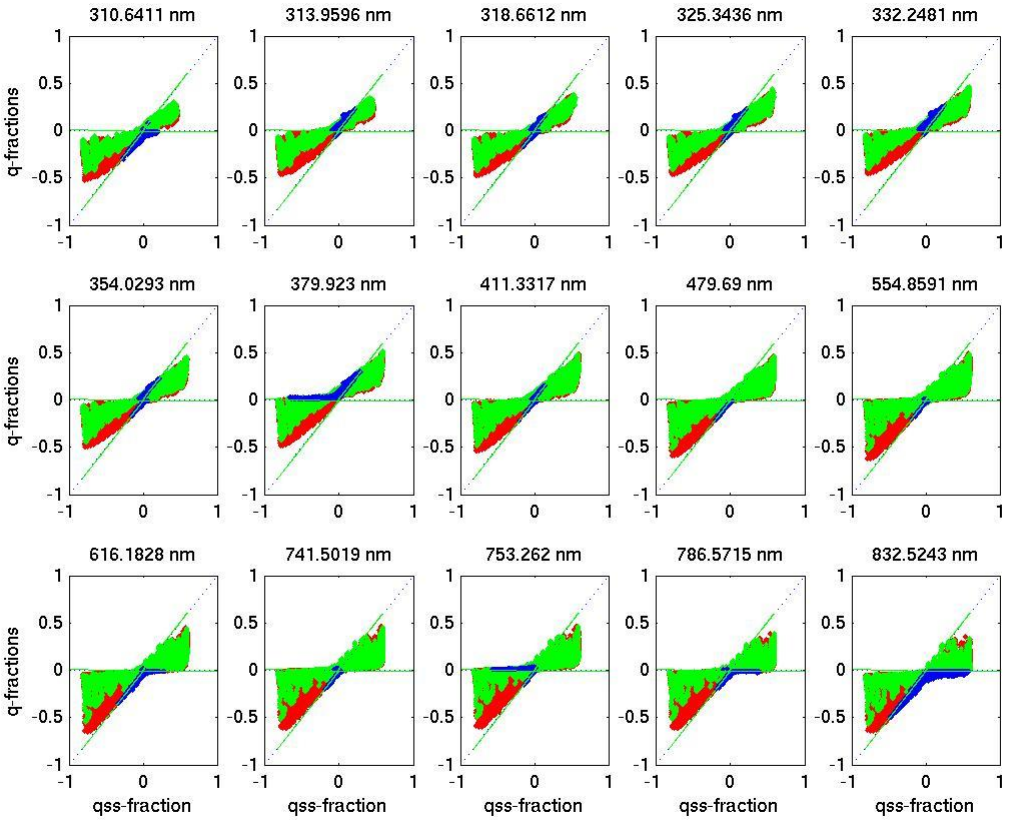

Figure 14: Limiting Atmosphere plot as for Figure 13 but based on the new spectral calibration scheme used from PPF 3.8

Figure 15 displays the reduction in Stokes fractions flagged as bad (due to the limiting atmosphere criterion) over the orbit for the old PPF 3.7.0. Note that the q-fractions in the middle panel are predominantly flagged as "bad" for regions with low single-scattering Stokes fractions. The reason for this might be an insufficient characterisation of the U polarisation component (45° polarised light) of the PMDs using ζ from the key-data, which lacks a characterisation of its viewing angular dependence (see 3.1.2) and is currently scaled by the ratio of the single scattering value of u (U/I) and q which is undetermined as q_{SS} approaches zero. The impact of the latter on the results is still to be characterised in the framework of the RAO GOME-2 polarisation study currently carried out by SRON. The new spectral calibration scheme already improves the situation for the old band definitions as shown in Figure 15.

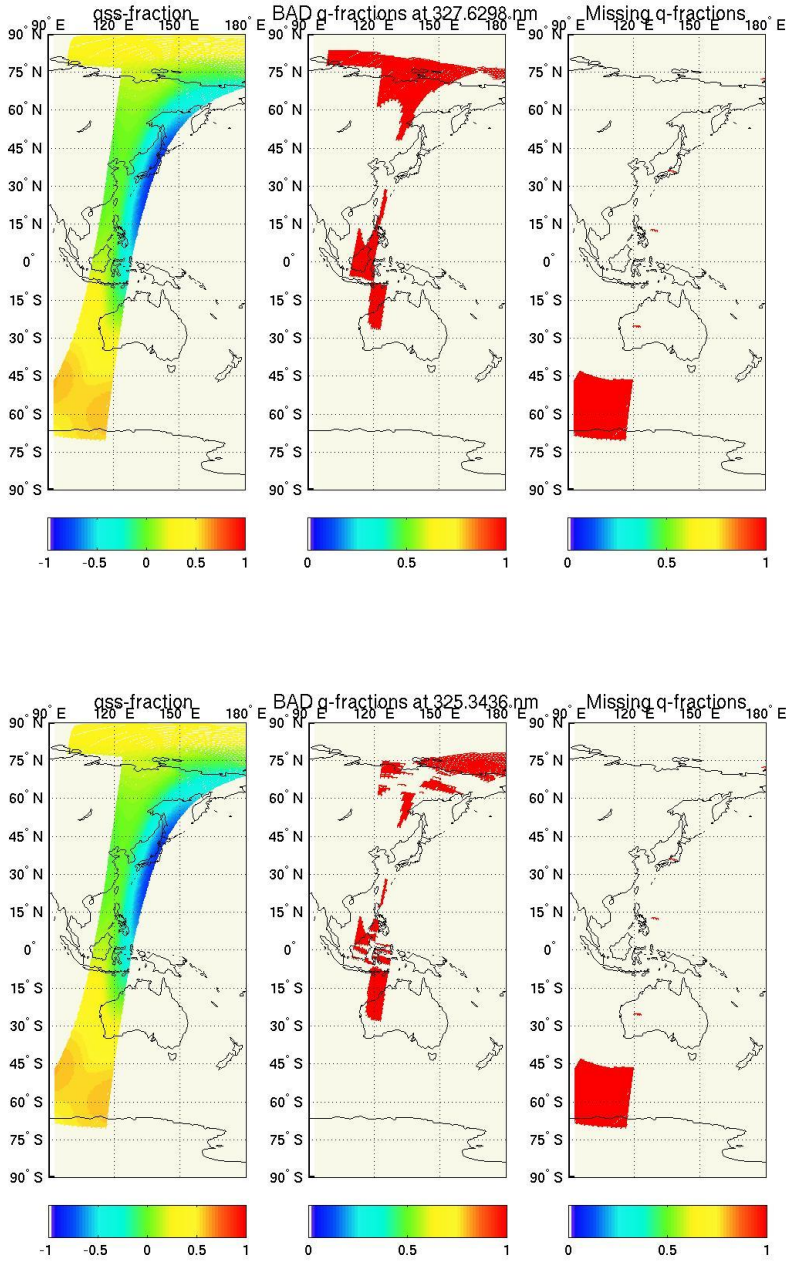

Figure 15: Changes in Stokes fractions flagged as "bad" (middle panel; due to limiting atmosphere criterion) over one orbit. The left panels show the single-scattering equivalent Stokes-fraction values and the right panels missing Stokes fractions (e.g. due to increasing signal-to-noise in the polar regions). The upper row denotes results from the old processor version 3.7.0 and the lower panels from the new one 3.8. The results are based on the old PMD band definitions v1.0.

Stokes fractions have been calculated for the test orbit for special geometries only. These special viewing geometries over the orbit are selected such that the Stokes fraction q approaches zero independent of the degree of linear polarisation of the reflected light. Note

that only cloud-free situations are taken into account (even though the degree of polarisation for cloudy scenes should also be low, the exact amount of reduction is difficult to quantify) but other influences from multiple scattering by aerosols etc. can also influence the results.

Figure 16 shows Stokes fractions for special viewing geometries again for both cases, employing the old and new spectral calibration schemes. The results clearly indicate a significant shift towards zero for close to all wavelengths. Remaining differences can be expected because of the use here of the unshifted on-board band definitions v1.0. Note that the largest deviations are around 380 nm and in the IR. This effect can also be observed in the Limiting Atmospheres plots above.

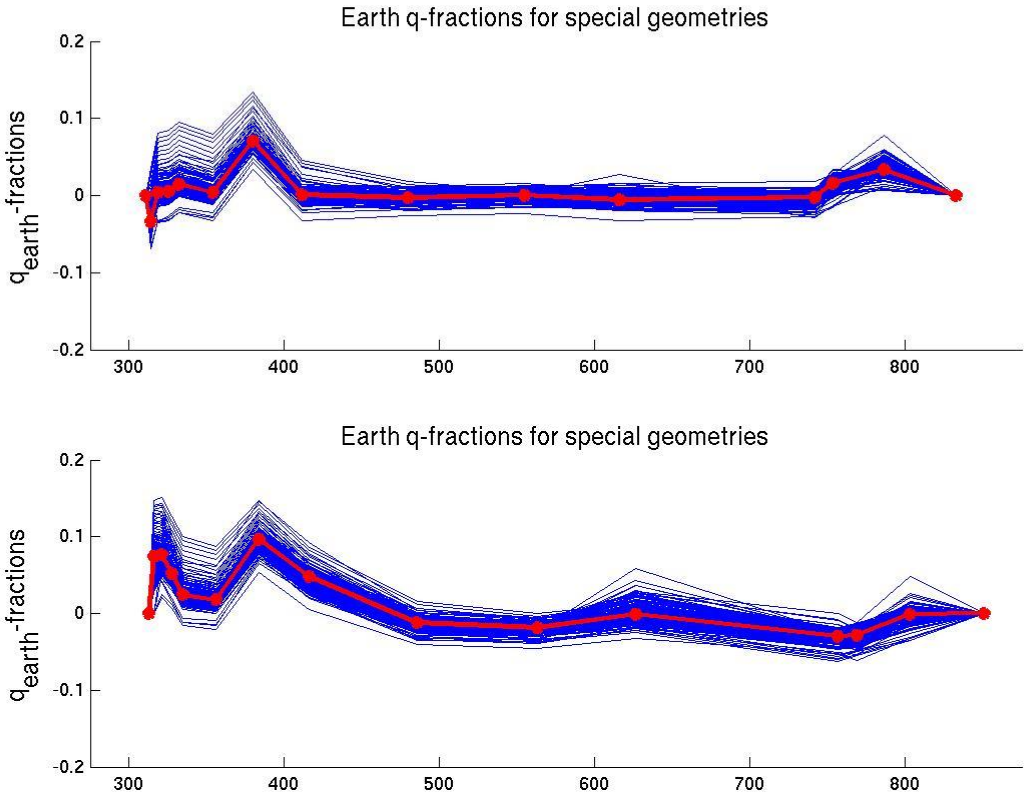

Figure 16: Stokes fractions for special viewing geometries (where q should be close to zero) over one orbit for PPF 3.8 (upper panel; new scheme) and PPF version 3.7.0 (lower panel; old scheme)

Figure 17 shows the same as Figure 16 but for the PMD raw read-out mode where all PMD detector pixels are transferred but however at a much poorer temporal resolution. Again, improvements for the new spectral calibration scheme are evident for the UV and IR region.

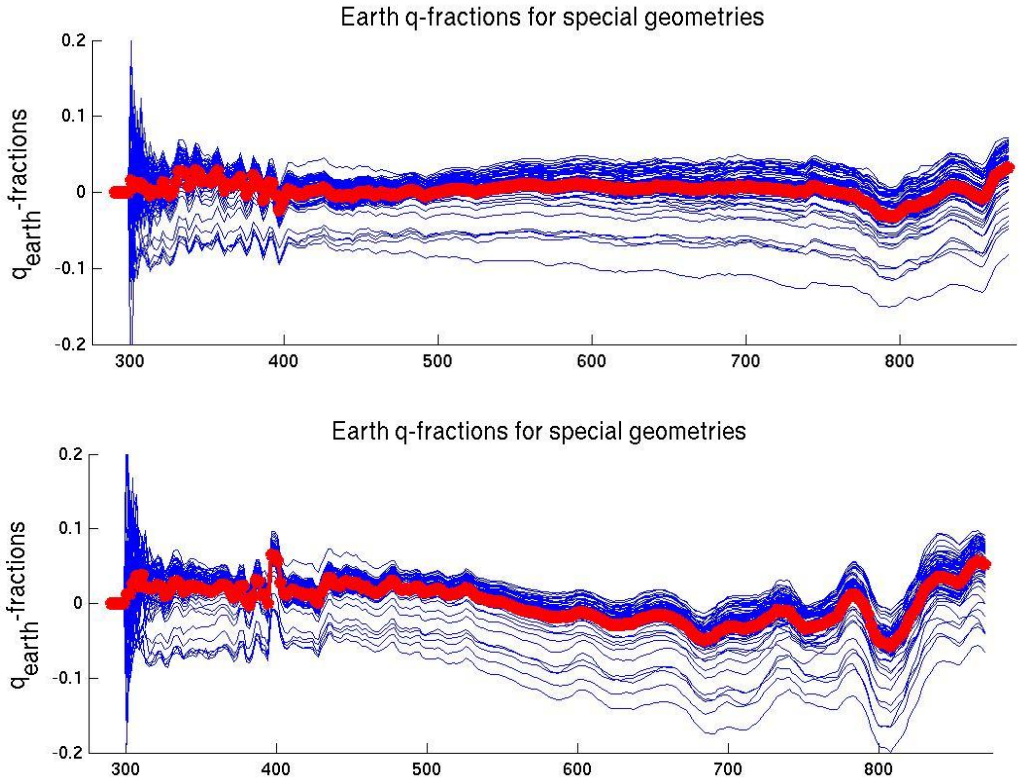

Figure 17: Same as Figure 16 but for PMD RAW read-out mode

Finally, Figure 18 shows the impact of the viewing angle on special geometry Stokes fractions. The impact of improving the spectral calibration is a shift towards 0 as is evident from the previous results. In addition there seems to be a slight improvement with respect to VZA dependence with 3.8 being less dependent especially for the visible and IR regions.

2.7 Impact of New Band Definitions v3.0 on PMD Calibration

During a one-day period on 6 February 2008 a test upload of the new PMD band definitions v3.0 was carried out. The processor version to derive level 1B data used here is 3.9 comprising all changes on spectral calibration for PMDs as laid out before. This version also solves a technical issue occurring during upload of the new PMD band definitions (with respect to PPF 3.8). The following results show the impact on Stokes fraction using the new PMD band definition v3.0. The results should be compared with those from the previous section for updated spectral calibration in order to judge the further improvement of the data due to the better co-registration of the new PMD band definitions.

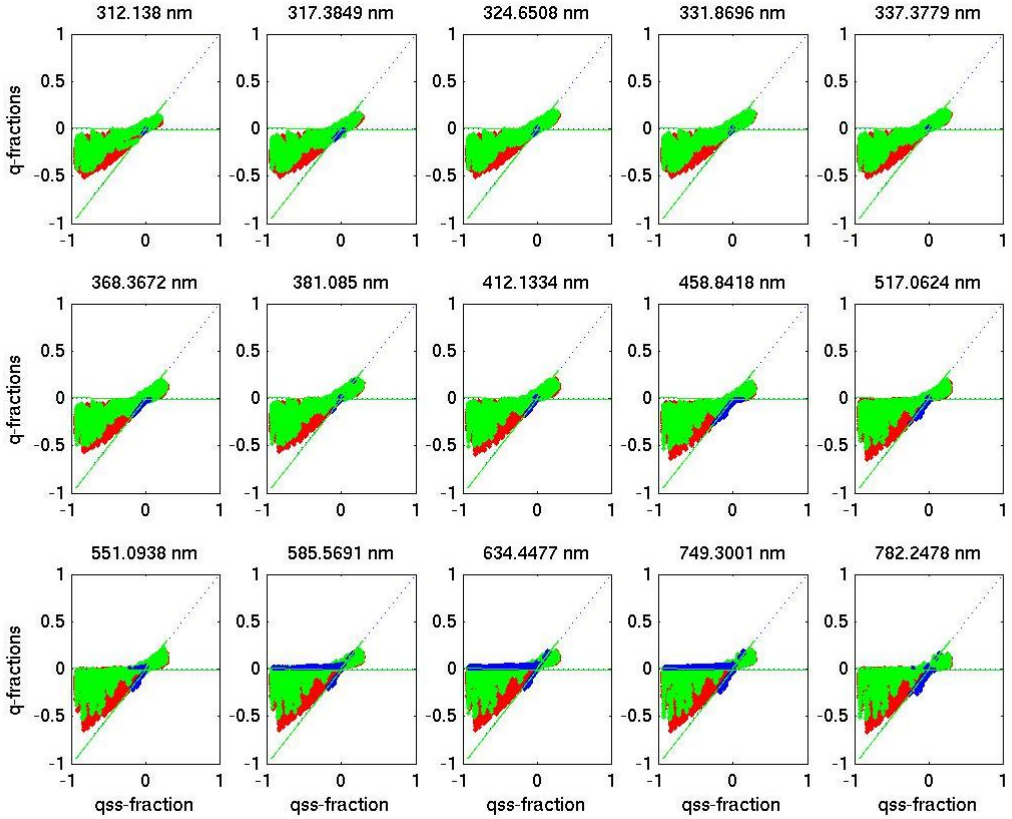

Figure 18: Limiting Atmosphere plot for all PMD bands derived Stokes fractions using the new spectral calibration scheme and based on new PMD band definitions v3.0. Green dots indicate back viewing, red forward viewing and blue dots fall outside the valid ranges defined by the limiting atmospheres.

The new band definitions show an overall improvement of Stokes fraction quality (fewer blue outliers) and a significant improvement for the UV (Figure 18 cf. Figure 13). This is also clearly visible when looking at Stokes fractions for special geometries (Figure 19 cf. Figure 16).

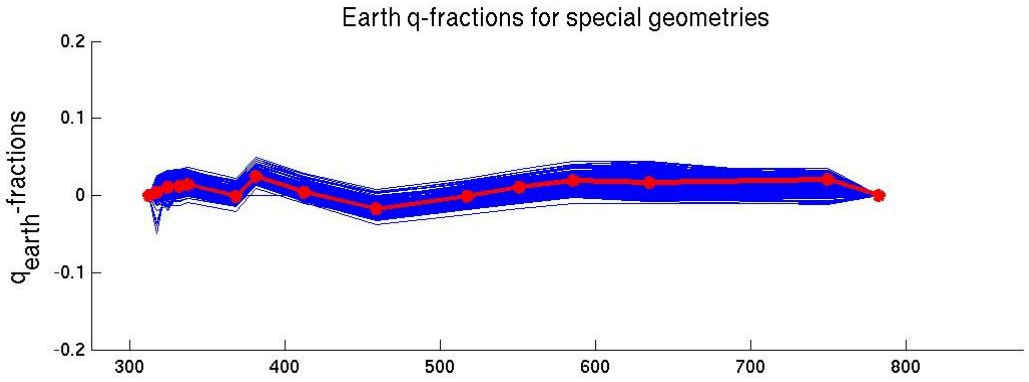

Figure 19: Stokes fractions for special viewing geometries (where q should be close to zero) over one orbit for new spectral calibration scheme and based on new PMD band definitions v3.0

3 PMD SIGNAL CALIBRATION

3.1 Remaining Stokes Fraction Spectral Offset and its Dependence on Viewing Angle and Time

It has been reported by several independent users of GOME-2 level 1B data that there is a viewing angle-dependent bias in retrieved geophysical data products, such as minimum reflectivity, O_3 and NO_2 total columns, particularly for cloud-free situations. As clouds tend to depolarise the scattered radiation field, the association with degree of cloudiness indicates a potential problem in the polarisation correction. The observed viewing angle dependence also varies with spectral region of interest, time of year and also over the mission life-time. This issue has been investigated by analysing the viewing angle dependence of Stokes fractions for special geometries (which should be very close to zero independent of the atmospheric state). A similar independent study has been carried out in parallel by the PMD study group led by SRON [RD1]. From both independent studies a time, wavelength and viewing angle-dependent bias has been observed for special-geometry Stokes fractions. Figure 19 shows the spread of special geometry Stokes fractions for one orbit where the mean value is shown by a red solid line and the blue lines indicate the spread with viewing angle. The residual error in the Stokes fractions, and therefore the polarisation correction, is thus composed of a mean spectrally-dependent offset with additional viewing angle dependence. This is the status following upgrade of the PMD band definition to version 3.0 and implementation of the new spectral calibration scheme.

Stokes fractions for special geometries derived from a reprocessed orbit 3372 (14 June 2007) using processor version 3.8.5, which includes all updates to the spectral calibration for PMDs as discussed earlier, indeed show a viewing angle dependence varying with wavelength and largest in the UV region. Figure 20 shows the viewing angle dependence of Stokes fractions for three different wavelengths showing large deviations particularly for East viewing geometries (negative viewing angles).

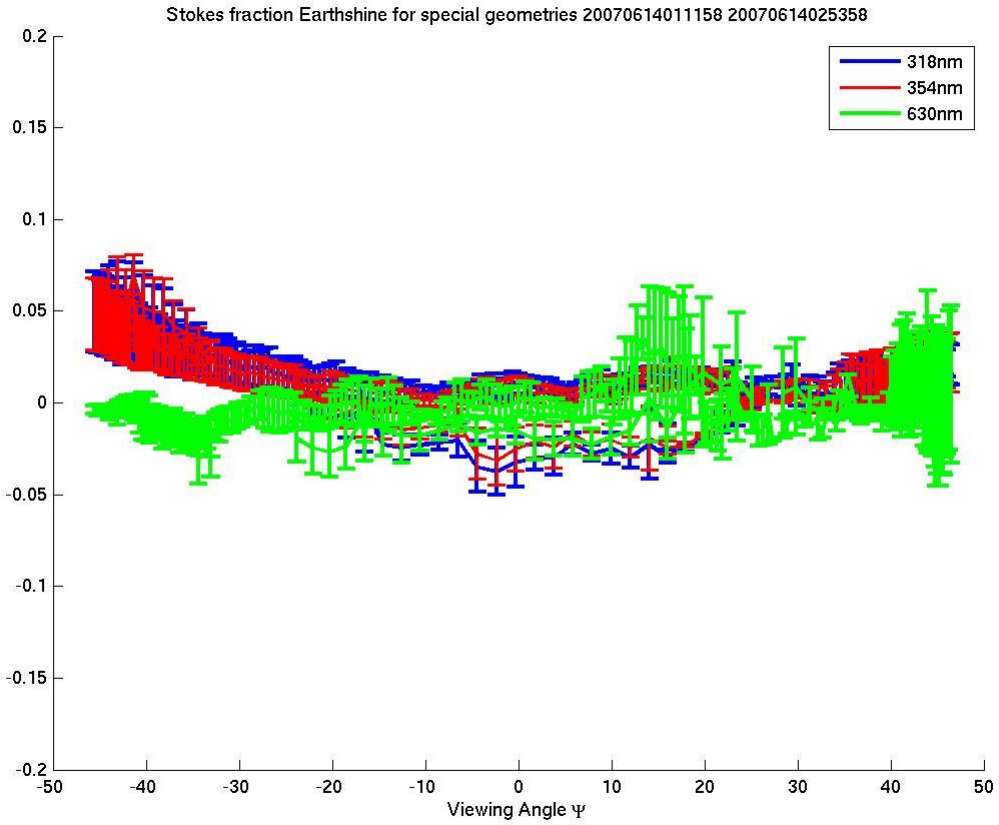

Figure 20: Stokes fractions for special viewing geometries (where q should be close to zero) over one orbit showing dependence on viewing angle. The error bars indicate the 1σ statistics on the mean.

3.1.1 Viewing Angle Dependence of Polarisation Sensitivity to Linear Polarised Light (χ)

It is expected that this observed viewing angle dependence is related to a difference between the on-ground key-data characterisation of the angular dependence of the polarisation response to linear polarised light, characterised by χ (PGS 6.1 [AD0] 5.2.3) and the in-flight situation. The otherwise quite complex relationship between the signals S_p and S_s from PMD P and S, the Stokes fraction q, and the MMEs (including χ) for PMDs, becomes very simple in the case of special geometry viewing situations for which we may assume q=0 (Eq. 229, PGS 6.1 [AD0]) and which then leads to the relationship

$$M^{1}_{S/P} = \frac{S^{S}}{S^{P}}. \qquad \textbf{Equation 1}$$

The relative radiometric response of PMD S to P ($M^1_{S/P}$) is a function of α, β, γ and χ (see Section 2.4.2.7) where χ describes the angular dependence of α and β [1] such that

$$\frac{S^S}{S^P} = \frac{\alpha\chi + \gamma}{\beta\chi + 1}. \qquad \textit{Equation 2}$$

During the on-ground calibration and characterisation campaign χ has been derived from FPA measurements but is assumed, as χ is understood to be a property of the scan mirror, to be applicable to PMDs also (see Appendix C). In order to test the validity of this assumption TNO have used available on-ground calibration measurements from the PMDs to derive a PMD-specific value of χ (hereafter χ_{PMD}) [RD4]. This has shown that the on-ground value for χ_{PMD} is predominantly consistent with the value derived on-ground for χ from FPA data[2]. There are some small residual differences attributed to an error in the FPA calibration measurements that have also been identified when comparing χ modelled from in-flight data to χ derived during the on-ground calibration and characterisation campaign.

In addition, the final report of the GOME-2 polarisation study issued by SRON [RD1] showed that the spectral dependence of the observed offsets is relatively stable based on 1.5 years of observations – see Section 2.7 and Figure 19 in this report, as well as concluding remarks of [RD1].

In contrast, over a period of one year, the viewing angle dependence shows a seasonal variation and a weaker but nevertheless significant long-term trend. Note that degradation is only expected to affect Stokes fraction quality in the case of a *differential* degradation between P and S signals (cf. Eq. 229, PGS 6.1 [AD0]) e.g. because of a differential throughput degradation. Figure 21 shows the differential degradation between P and S over more than two years of acquired solar mean reference PMD spectra measurements. A strong apparently seasonal component and a weaker (but increasing especially in the UV) long-term differential degradation component can be seen.

[1] Note that χ is also used in the derivation of the polarisation sensitivity of FPAs and PMDs to linear polarised light μ_2, [AD0] 5.2.16.

[2] Stored in the POL_CHI key-data file and used for both FPA and PMD data in orbit until processor version 3.8; see also Appendix C for the complete history in handling χ and χ_{PMD} for processor versions 3.9 to 4.2.

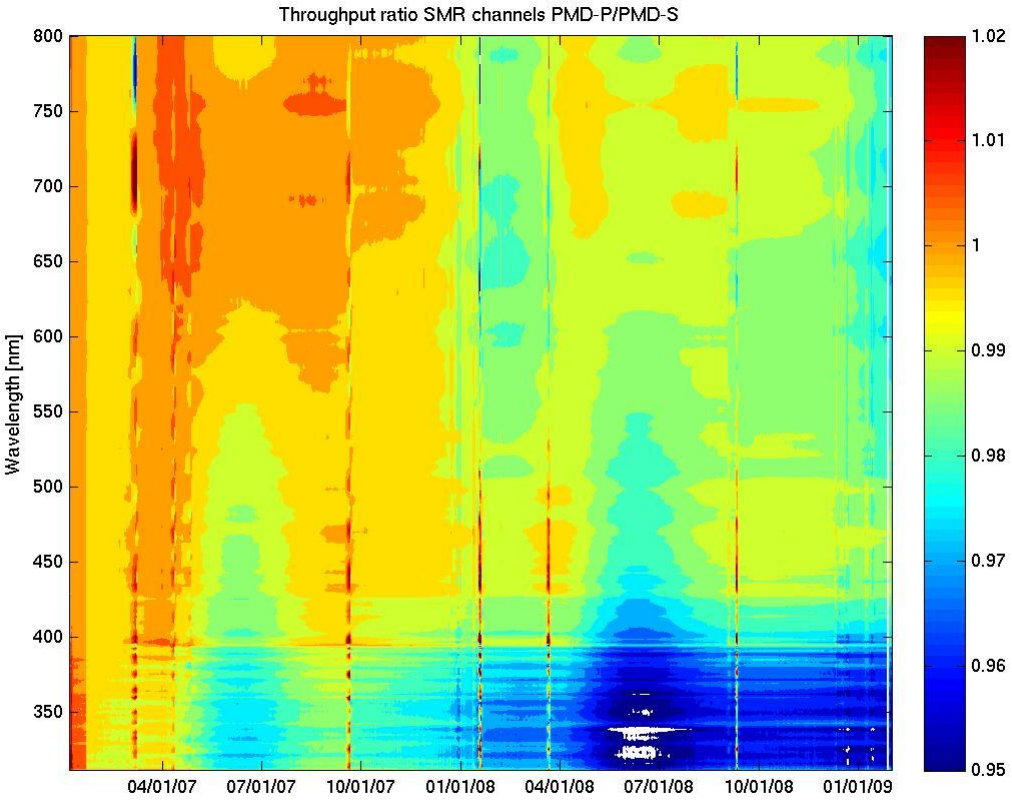

Figure 21: Differential throughput degradation between PMD-P and S signals relative to January 2007

From this we may conclude the following:

- A pre-flight/in-orbit change appears to have occurred, introducing a persistent offset in Stokes fractions for special geometries (and therefore most likely for all derived Stokes fractions).
- The viewing angle dependence of this offset has a strong seasonal component.
- There is a weak but non-negligible contribution of long-term *differential* degradation to the observed signatures. Long-term instrument throughput degradation issues are discussed in more detail in [RD3].

3.1.1.1 In-flight Correction of Observed Stokes Fraction Offset and Viewing Angle Dependence (PPF 4.3 and later versions)

Under the assumption that the offset and viewing angle dependence, as observed in Stokes fractions for special geometries, is applicable to all derived Stokes fractions, and therefore will impact the quality of the polarisation correction (and subsequently the overall quality of level 1B data), the following in-flight correction scheme has been developed, tested and implemented with PPF version 4.3 and higher versions.

The scheme developed offline and the results shown here are based on the acquisition of approximately one day of PMD S and P signals for band read-out data (nominal Earthshine viewing data). The exact acquisition time is based on the accumulation of available P and S signals, satisfying pre-defined quality criteria, for special geometry situations. Once the number accumulated exceeds a certain threshold (i.e. sufficient statistics have been acquired on a one-day time scale), the ratio of S over P is averaged in time for all wavelengths and viewing angles.

Figure 22 shows the number of measurements acquired within one day of data accumulation and as a function of wavelength and viewing angle. Note that the PMD-S and P data are interpolated from the 15 band values to a common spectral grid (MME grid) of 279 points[3] and to a common viewing angle fixed grid of 193 angles (equivalent to the PMD read-outs in one forward scan) for this exercise in order to further improve co-registration of PMD-S and P data and in order to allow for slight changes in the actual viewing angles when subsequently applying a correction.

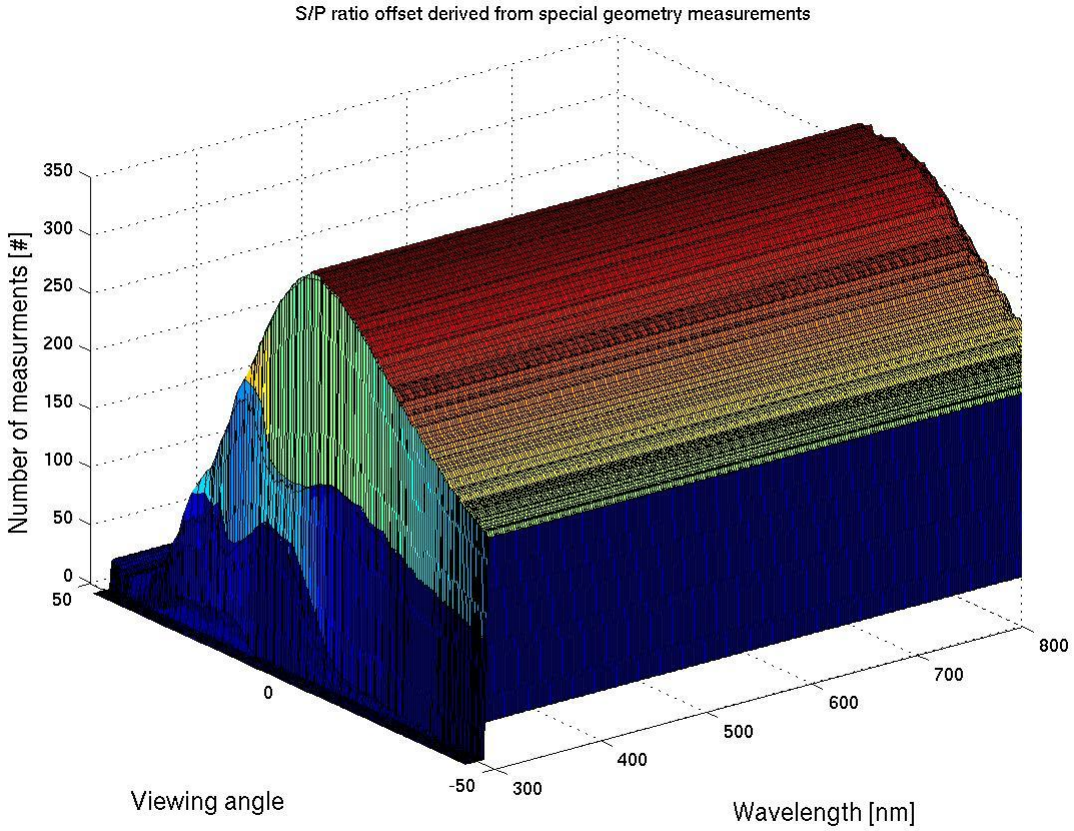

Figure 22: Number of special geometry S and P signal measurements acquired offline per wavelength and viewing angle during one day in March 2009. Note that there are many more special geometry situations found in the East (forward scattering) and around nadir than in the West (backward scattering) for a morning orbit viewing geometry (see also [RD1]).

[3] This is an intermediate step before calculating q-fractions on the MME grid and then interpolating back to the original band data grid.

From these measurements an average offset Δ for the time period under analysis (approximately two days) is derived online by the PPF as

$$\overline{\Delta} = M^1_{S/P} - \frac{S^S}{S^P}, \qquad \textit{Equation 3}$$

as a function of both fixed wavelength and viewing angle grids. The derived correction is to be understood as a dynamic correction to $M^1_{S/P}$.

Figure 23 shows the result for the time-averaged Δ on 9 March 2009 (one full day of data) as a function of wavelength and viewing angle.

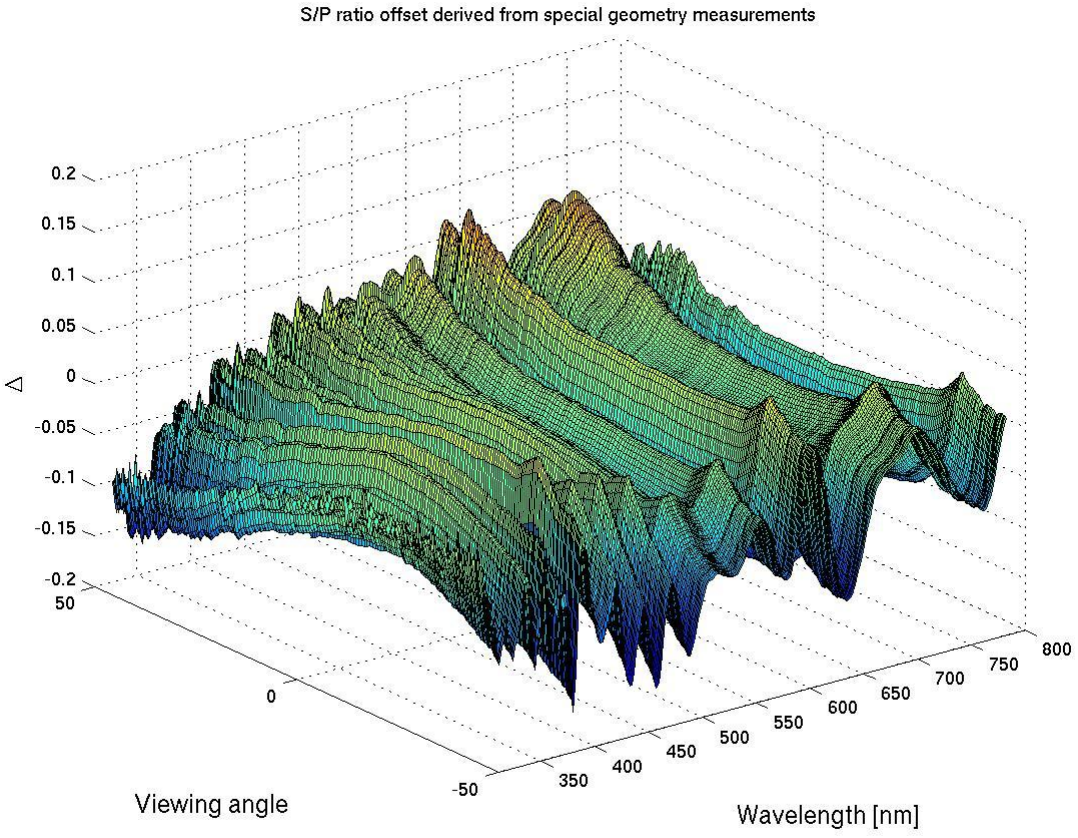

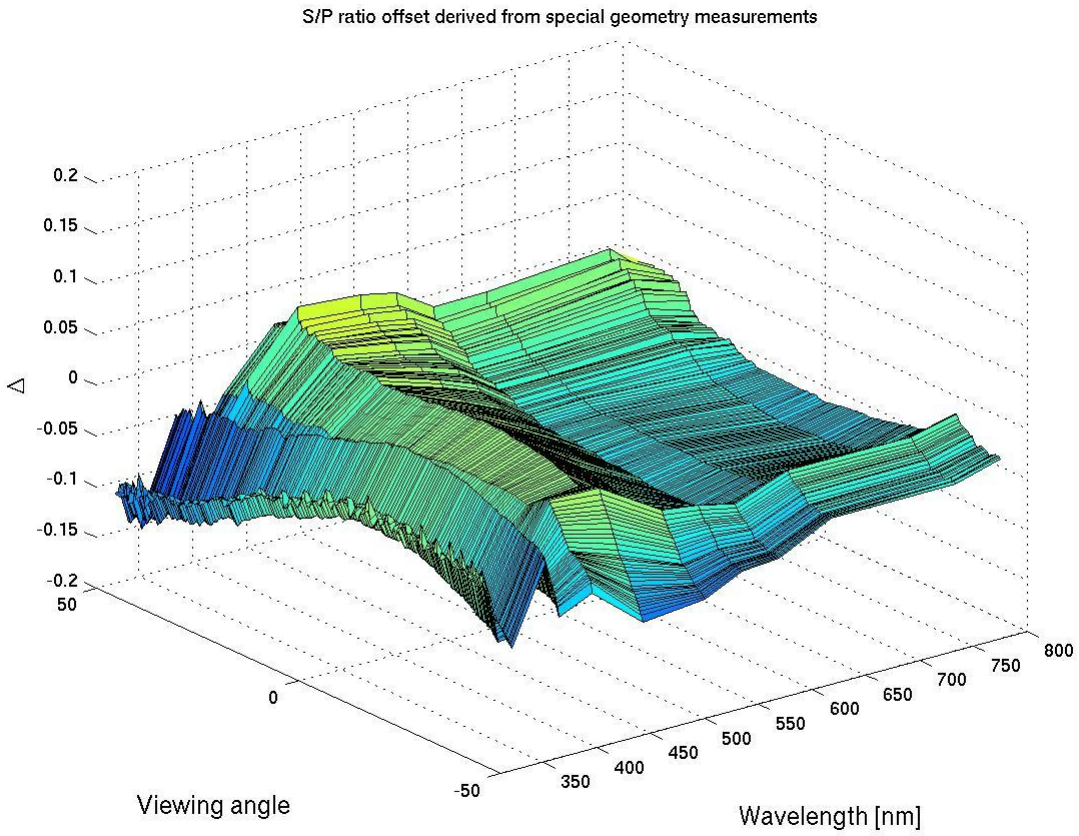

Figure 23: Δ (as defined in Equation 3) derived for 9 March 2009 and displayed on the intermediate MME wavelength grid (279 spectral points, upper panel) and interpolated back to the original 15 PMD band spectral grid (lower panel)

Figure 24 shows the same time-averaged offset Δ for 9 March 2009 but now averaged over viewing angle (red line) to be compared with the offset shown in Figure 19. These are provided on the MME grid (upper panel) and then interpolated back to the original 15 Stokes fraction band wavelengths (lower panel). Note that Figure 19 and Figure 24 show data from different dates (March 2009 and June 2007). Nevertheless the Δ derived in March 2009 matches the offset from 2007 quite well with the exception of a sign difference resulting from the definition of Δ.

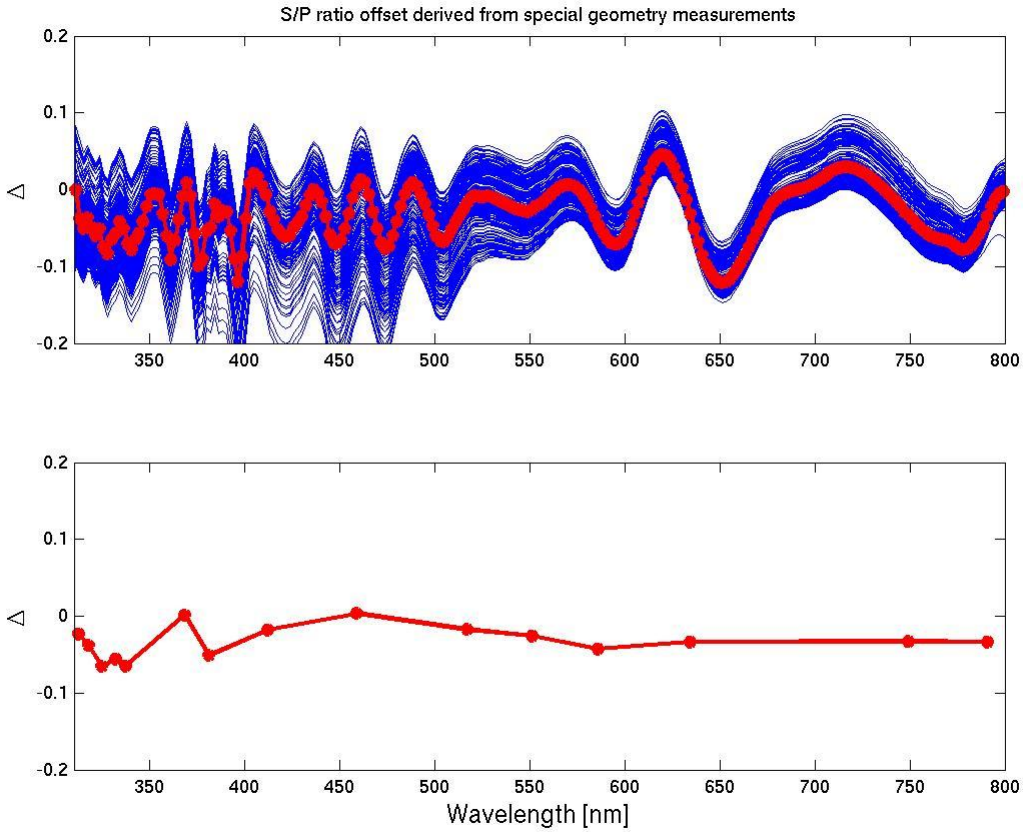

Figure 24: Δ (as defined in Equation 3) derived for 9 March 2009 and displayed on the intermediate MME wavelength grid (279 spectral points, upper panel) and interpolated back to the original 15 PMD band spectral grid (lower panel). The red line shows the average of all viewing angles which can be compared (with the exception of the sign difference) to the offset shown in Figure 19.

After the acquisition of a maximum of two days of data and accumulation of a minimum of six valid and quality-checked measurements per viewing angle, the matrix displayed in Figure 23 is written to the GOME_COR auxiliary file and applied during the derivation of Stokes fractions q by correcting the PMD relative radiometric response key-data[4] by

$$\overline{M^{1,c}_{\measuredangle_P i,\Psi_j}} = \overline{M^{1}_{\measuredangle_P i,\Psi_j}} - \Delta^{c}_{i\Psi_j}, \qquad \textit{Equation 4}$$

where *i* is the index for the wavelength grid (here MME grid) and *j* the read-out index corresponding to the actual viewing geometries (viewing angles).

The corrected signal response ratio $\overline{M^{1,c}_{\measuredangle_P i,\Psi_j}}$ is finally used for the derivation of all (!) Stokes fractions q_{ij} by applying

[4] See Eq. 229, PGS 6.1 [AD0]

$$q_{ij} = \frac{\overline{M^{1,c}_{\left(P\right)ij,\Psi_j}} - \frac{S^S_{ij}}{S^P_{ij}}}{\left(\mu^2_{ip,\Psi_j} + \mu^3_{ip,\Psi_j}\frac{u_{SS,\Psi_j}}{q_{SS,\Psi_j}}\right)\frac{S^S_{ij}}{S^P_{ij}} - \left(\mu^2_{is,\Psi_j} + \mu^3_{is,\Psi_j}\frac{u_{SS,\Psi_j}}{q_{SS,\Psi_j}}\right)\overline{M^{1,c}_{\left(P\right)ij,\Psi_j}}} \qquad \textit{Equation 5}$$

where Ψ_j is the viewing angle corresponding to read-out j (cf. Eq. 229, PGS 6.1 [AD0]).

This scheme is applied for both Stokes fractions q_{ij} derived on the PMD read-out resolution (256 read-outs per viewing) and for Stokes fractions q_{imn} mapped on the FPA read-out grid (depending on actual integration time, currently maximal 32 read-outs per viewing; see Eq. 231, PGS 6.1 [AD0]).

3.1.1.2 Offline Validation of New PMD Signal Ratio Correction Scheme (for PPF 4.3 and Higher Versions)

Stokes fractions q_{ij} for special geometries have been derived offline for all viewing geometries and read-outs available from one orbit on 13 January 2009. Stokes fractions q_{ij} calculated using the on-ground calibration key-data, uncorrected, are compared to those calculated applying the PMD signal ratio correction scheme as laid out in the previous section. Note that Δ_{ij} has been derived from data of 9 March 2009, and for the offline calculations shown here the original key-data delivery for χ (where $\chi_{PMD}= \chi_{FPA}$ used until processor version 3.8) has been used as input to the process. Δ_{ij} is subsequently generated online and used to correct these data for the derivation of the corrected Stokes fractions q_{ij} (see also Section 3.1.1).

Figure 25 to Figure 27 show Stokes fractions averaged over one orbit for 13 January 2009 **without** any PMD signal-response key-data correction applied. The offset in wavelength and viewing angle space is clearly visible.

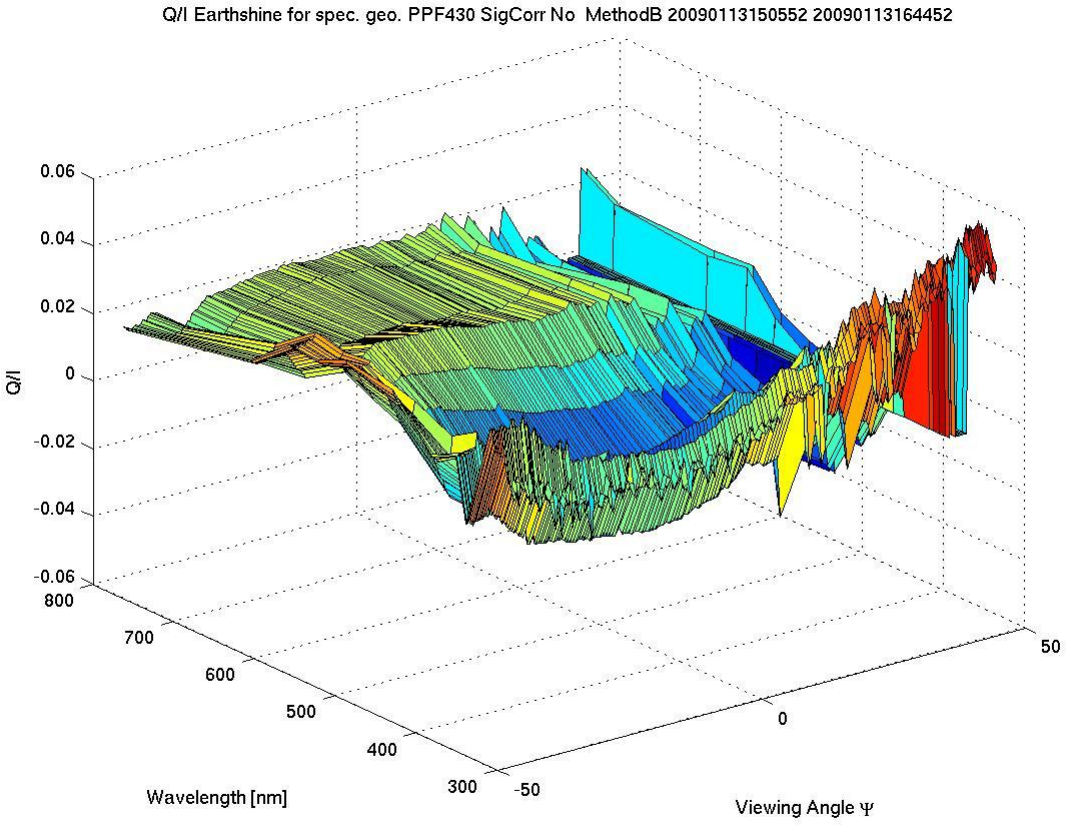

Figure 25: Average Stokes fraction for special viewing geometries q_{ij} for 13 January 2009 without correction to the relative radiometric response of PMD S and P. The original χ_{PMD}= χ_{FPA} key-data has been used for this orbit.

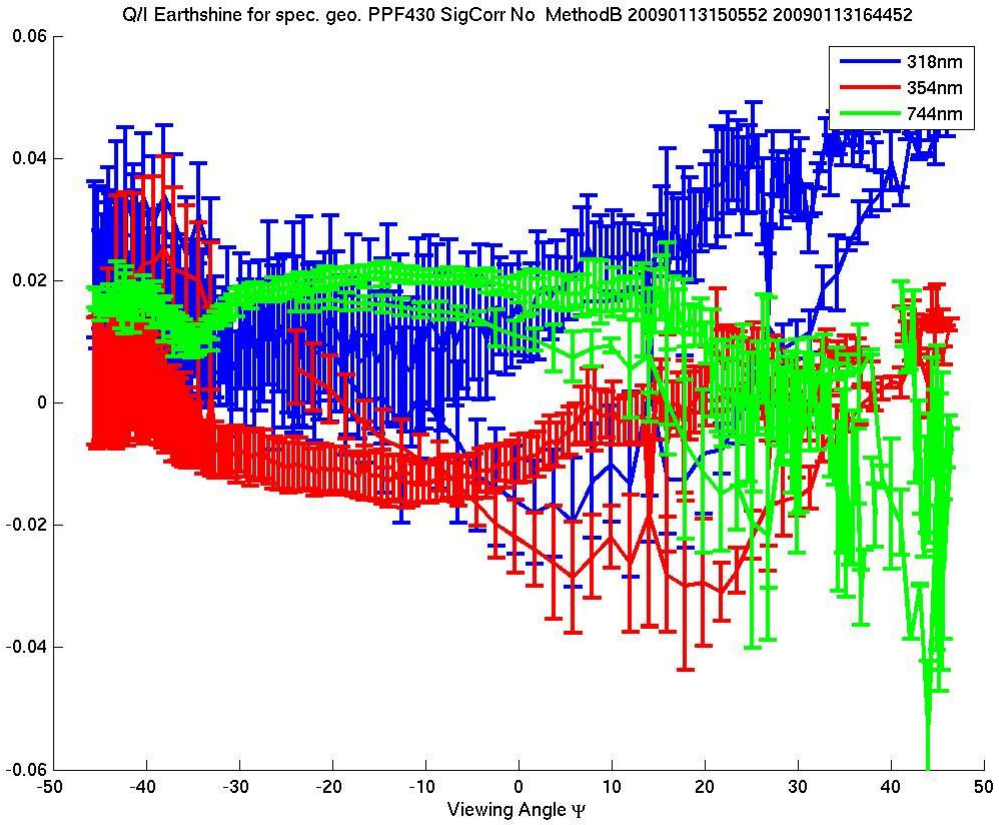

Figure 26: One-day average Stokes fraction q_{ij} on 13 January 2009 without correction to the relative radiometric response of PMD S and P for three selected wavelengths (cf. Figure 34 or Figure 35 in Appendix C). The original $\chi_{PMD} = \chi_{FPA}$ key-data has been used for this orbit.

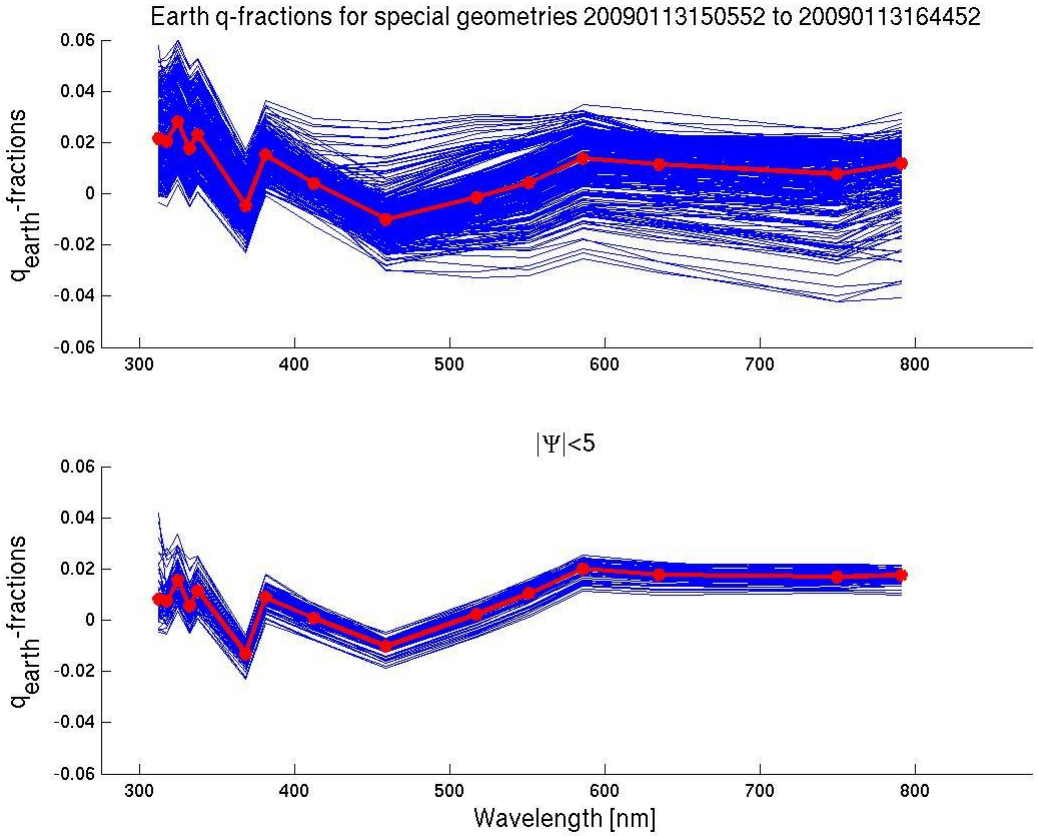

Figure 27: One-day average Stokes fraction q_{ij} on 13 January 2009 without correction to the relative radiometric response of PMD S and P for all viewing geometries (upper panel, blue lines) and for nadir viewing only (lower panel, blue lines). The red line shows the average over all viewing angles for both cases. The original χ_{PMD}= χ_{FPA} key-data have been used for this orbit. Note the difference in Stokes fraction scale as compared to Figure 19.

For a second run of the same orbit we derived the same parameters but now applying the PMD signal-ratio correction Δ_{ij} as derived in the previous section. Figure 28 to Figure 30 shows the corresponding results for the derived q_{ij} values with correction applied.

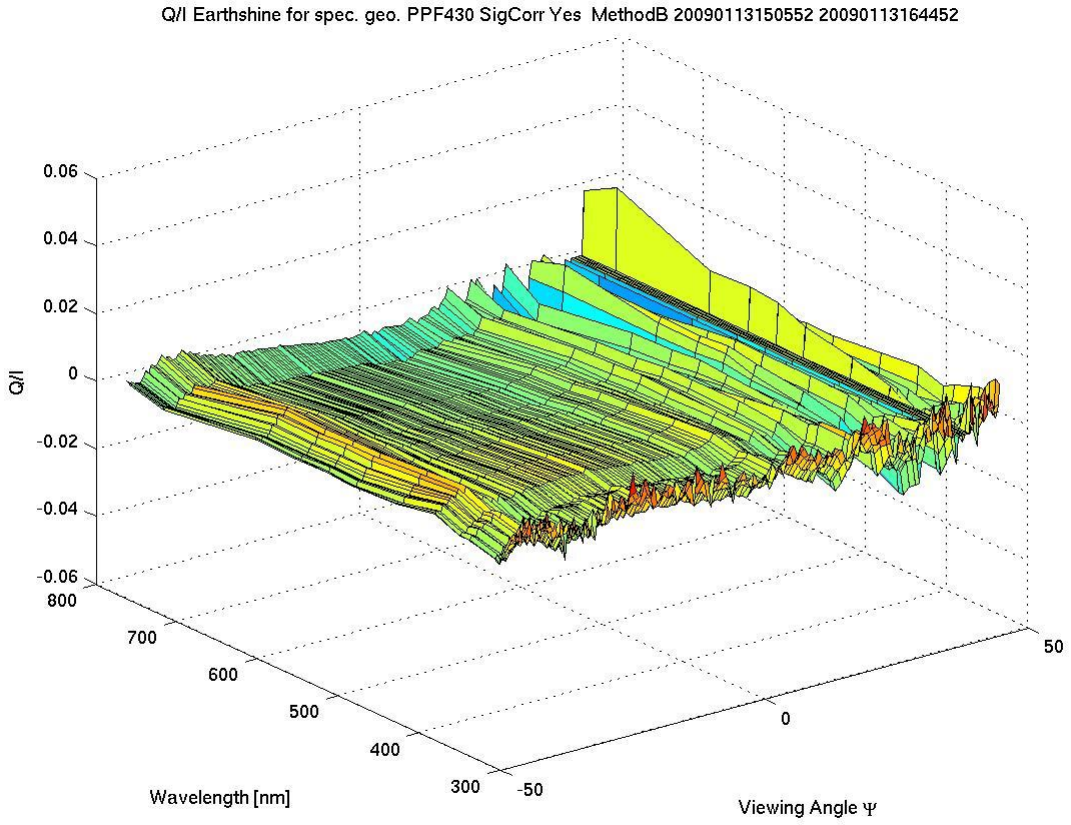

Figure 28: Same as Figure 25 but with correction to the relative radiometric response of PMD S and P turned on

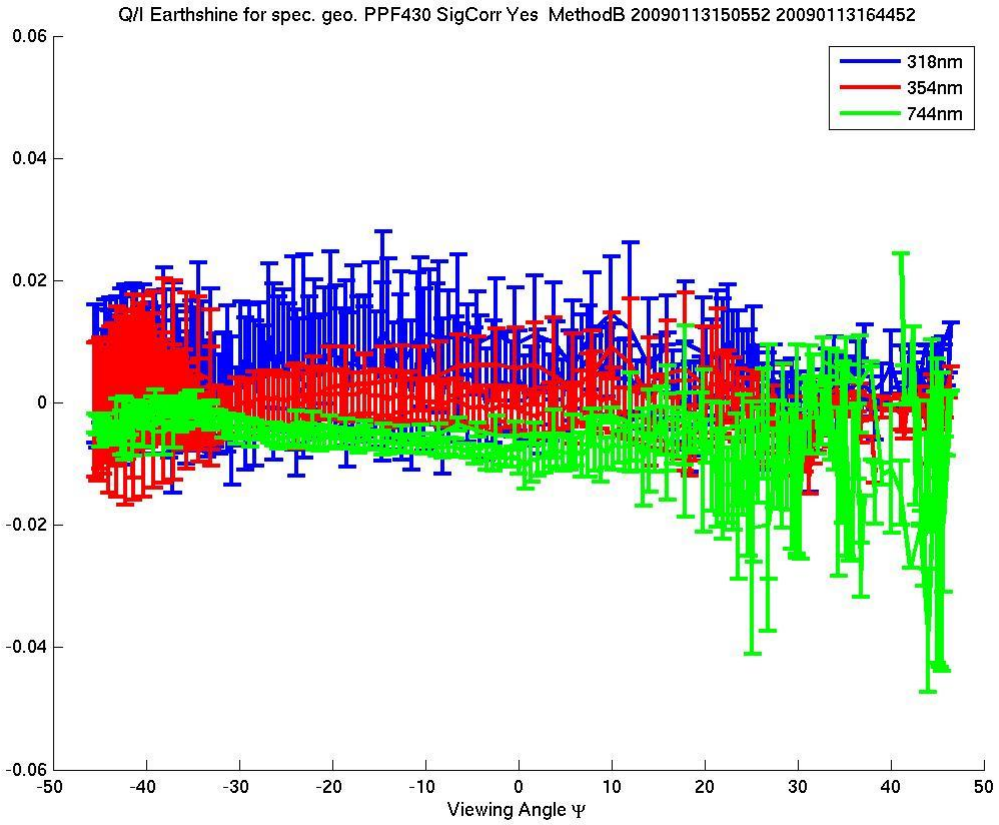

Figure 29: Same as Figure 26 but with correction to the relative radiometric response of PMD S and P turned on

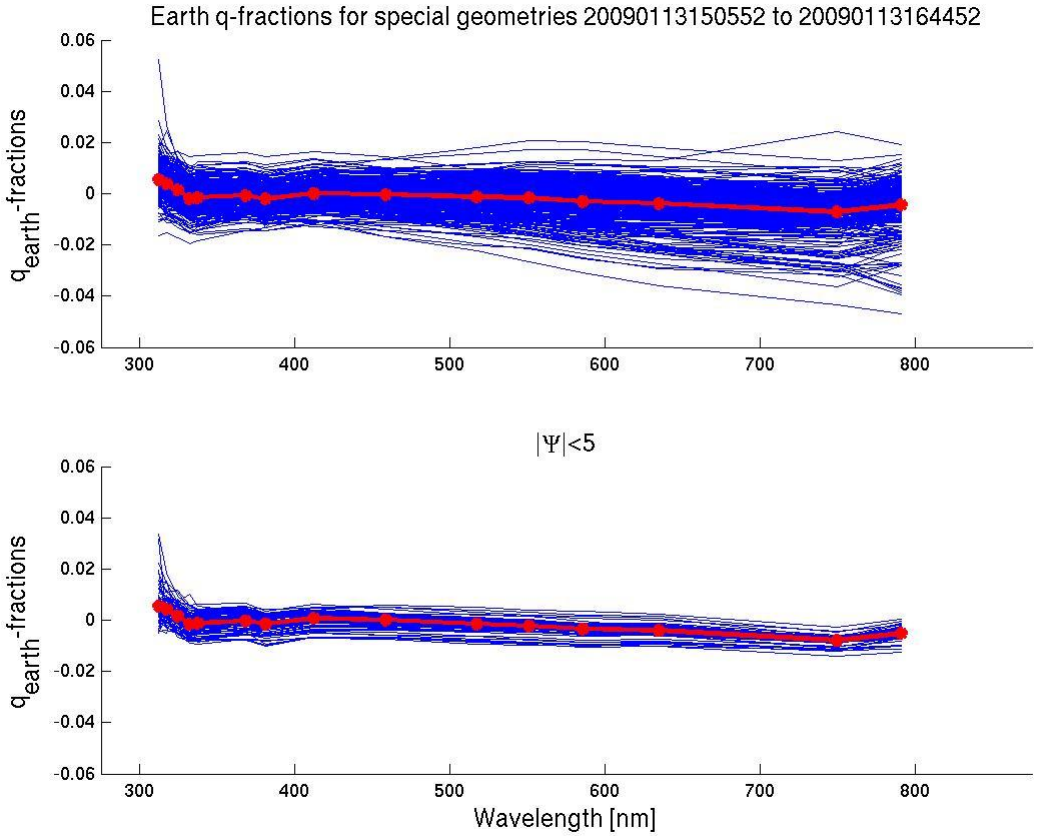

Figure 30: Same as Figure 27 but with correction to the relative radiometric response of PMD S and P turned on

From the above results we may conclude that the scheme for the correction of the relative radiometric response of PMD S and P significantly improves the quality of the derived Stokes fractions for special geometries and therefore (potentially) the overall quality of the derived Stokes fractions and level 1B FPA data, even using a correction Δ_{ij} which is two months apart in time from the corrected data.

3.1.2 Viewing Angle Dependence (χ) of Polarisation Sensitivity (ζ) to 45° Polarised Light

The calibration key-data ζ describes the sensitivity of the instrument to the Stokes parameter U (45° polarised light component of the Stokes vector). The angular dependence of ζ, i.e. χ_ζ, is not part of the calibration key-data pack delivery although from a physical perspective it was assumed to have a significant angular dependence. It was found, by examining the source code provided with the calibration key-data set, that the angular dependence of ζ was generated, but not delivered as a formal deliverable. This has been provided to EUMETSAT on an informal basis and is currently used in GOME-2 PPF 3.9. by adding the following file to the key-data package:

POL_CHI_ZETA.203.

χ_ζ is now applied in the following way during preparation of MMEs (cf. [AD0], Eq. 11)

$$\mu^3 = \frac{\zeta\chi_\zeta - 1}{\zeta\chi_\zeta + 1}. \qquad \textit{Equation 6}$$

This data should in future for all delta calibration activities be part of the formal calibration key-data pack (see also [AD4], Section 6.3).

The results of applying both χ and χ_ζ in the calculation of Stokes fractions for special geometry is shown in Figure 22. We find that the updated viewing angle dependence of Stokes fractions has significantly improved.

Note that for PPF 3.9 to PPF 4.3 (inclusive) the provided key-data for χ_ζ has been assumed to be valid (applicable) to both FPAs and PMDs. However, TNO pointed out in a technical report submitted to EUMETSAT in April 2009, that χ_ζ is not only a scan-mirror quantity but has some channel properties in it (see section 3.2. of the TNO report [RD6]). Consequently an informal delivery of the χ_ζ properties of PMDs has been made by TNO on 7 April 2009. The data have been validated by EUMETSAT and are contained in the following two key-data files:

POL_CHI_ZETA_PMD_P.203
POL_CHI_ZETA_PMD_S.203.

The reading and application of these new key-data files has been implemented with PPF version 4.4.0 in January 2010 and for later versions.

3.2 Stray-Light Correction for Polarisation Response Key-Data

Prior to the key-data specialist meeting, which took place on 3 September 2009 [RD7], TNO has reported that the application of stray-light correction during the derivation of key-data for polarisation response has not been turned on in the extraction program (this could be confirmed by EUMETSAT since in the respective delivery of the IDL code this option has also not been turned on). A corrected set of key-data have been re-delivered by TNO on 14 and 30 October 2009. After subsequent checks on the consistency of the delivered data with the EUMETSAT-derived versions of stray-light corrected data, the affected key-data have been updated and will be used in an updated CAL auxiliary file (version 1.08) starting with processor version PPF 4.4.0 and later versions. The following files have been corrected:

POL_ALPHA.203
POL_BETA.203
POL_GAMMA.203
POL_ETA.203
POL_ZETA.203

4 PLANNED IMPROVEMENTS TO PMD SIGNAL AND STOKES FRACTION QUALITY

There are outstanding issues on the calibration of PMD signals from solar measurements. An offset in the monitoring of solar Stokes fractions has been observed since the beginning of the mission. It is currently being investigated if this is the result of a deficiency in the key-data for the radiometric response of the calibration path. The consequence for the calibration of main channel data for solar reference measurements is yet to be decided.

APPENDIX A OFFLINE VALIDATION OF PPF 3.7.0 PMD DATA EMPLOYING NEW BAND DEFINITIONS V2.0

This Appendix employs level 0 data from orbit 5026 to 5037 measured during 8-9 October 2007, the period of the PMD band definitions v2 test upload. The processor version used is 3.7.0 **for all cases observed** running in the offline EUM TCE environment with GOME initialisation file version 1.17. The results compare key PMD measurement-derived parameters from the processing, such as Stokes fraction and P over S ratios, using the current **old** (SIOV v1) and the **intermediate** (GSAG 2) PMD band definitions.

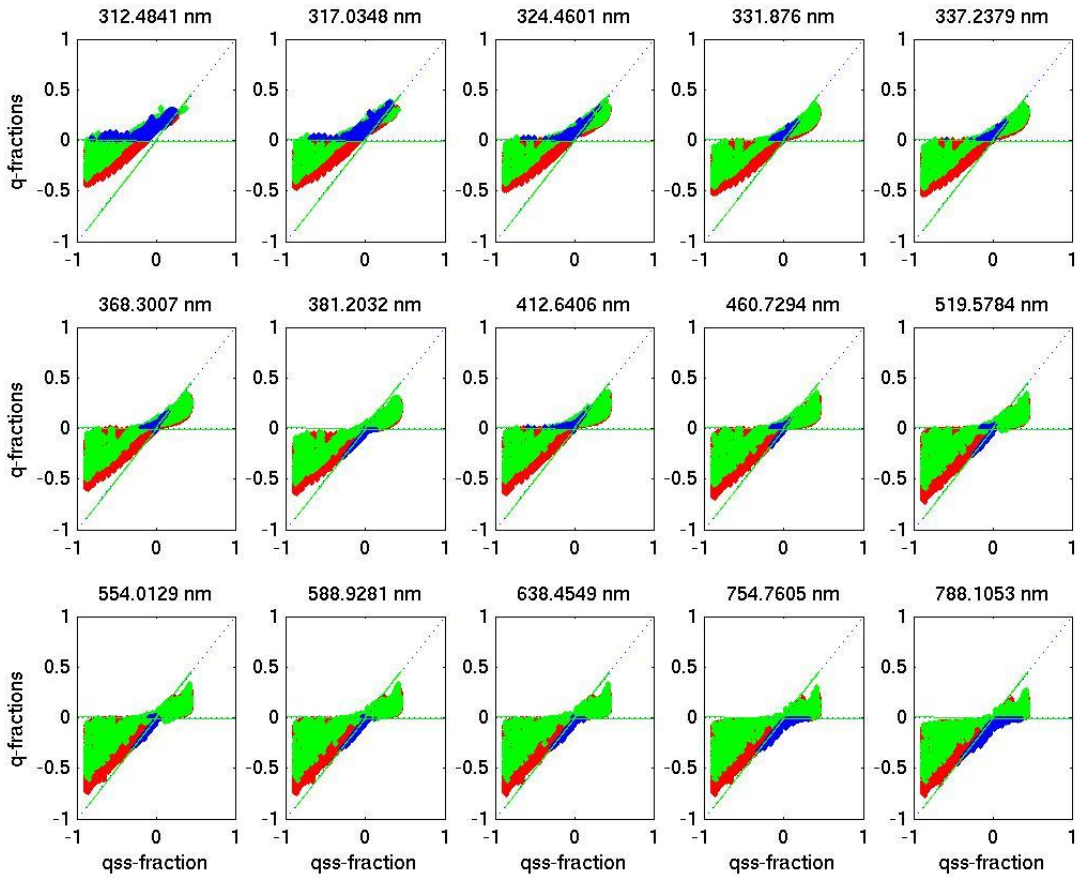

Figure 31: Limiting Atmosphere plot for all PMD bands derived Stokes fractions based on previous PMD band definitions v1.0. Green dots indicate back-viewing, red forward viewing and blue dots fall outside the valid ranges defined by the limiting atmospheres.

Figure 31 and Figure 32 show the results for PMD-derived Stokes fractions plotted over single-scattering Stokes fraction values (Limiting Atmosphere test). Green dots stem from back-viewing measurements, which cover forward viewing measurement results indicated in red. All blue dots fall outside the limiting atmosphere criterion and therefore indicate a degradation of the polarisation correction. When changing to the new PMD band definitions, the picture changes significantly (apart from the overall redistribution of band positions in wavelength) especially in the IR and UV. Whereas the IR generally improves, the UV is now

overshooting to some extent. The latter is a result of the long-term differential spectral shift between PMD P and S spectral calibration which is not accounted for by the processing (see Figure 21).

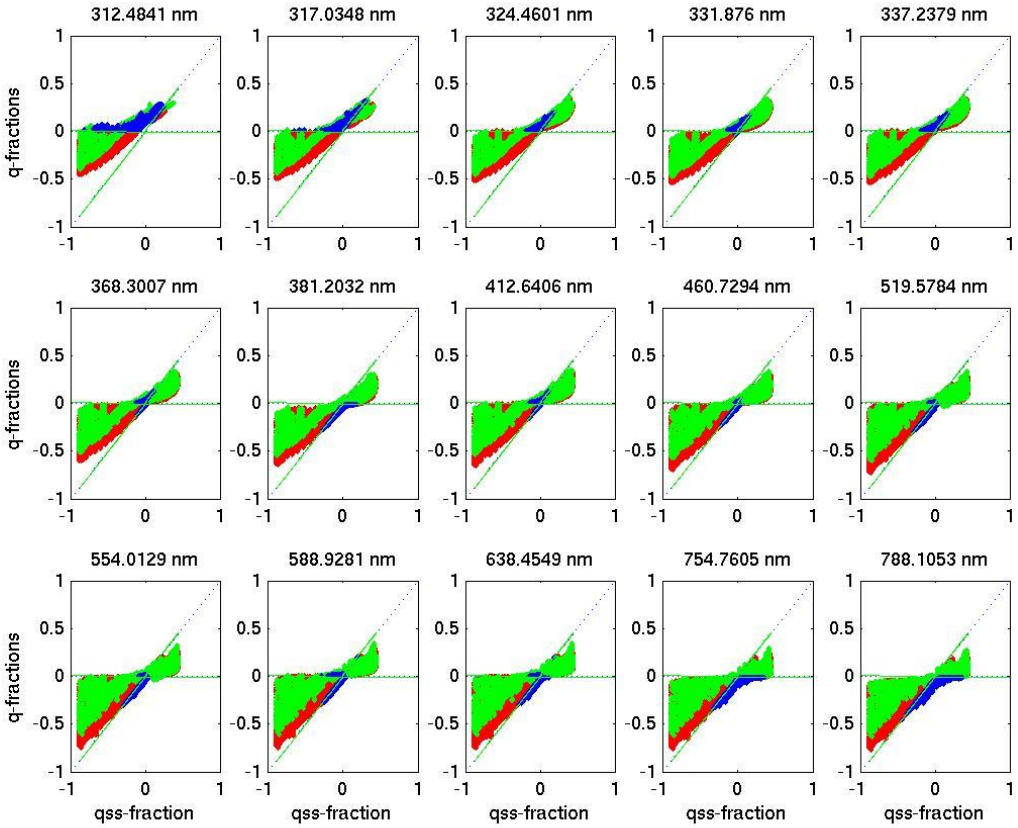

Figure 32: Same as Figure 18 but for new GOME-2 PMD band radiances based on the intermediate definitions (v2.0) as endorsed by GSAG

As mentioned already in Section 2.3, for processor version 3.7.0 a spectral interpolation scheme has been introduced in order to take into account the remaining shift between PMD P and S bands. The latter is applied for Figure 18 and Figure 19, i.e. the plots show the final quality of the Stokes fractions employing the new band definitions and using the new interpolation scheme.

Figure 33 displays the reduction in Stokes fractions flagged as bad (due to the limiting atmosphere criterion) over the orbit with respect to the old set-up. Note that the q-fractions in the middle panel are predominantly flagged as "bad" for regions with low single-scattering Stokes fractions. The reason for this might be an insufficient characterisation of the U polarisation component of the PMDs employing zeta (ζ) from the key-data, which currently lacks an angular dependence characterisation. The impact of the latter on the results is still to be characterised in the framework of the RAO GOME-2 polarisation study currently carried out by SRON. Both the new interpolation scheme and the new PMD band definitions already significantly improve the situation.

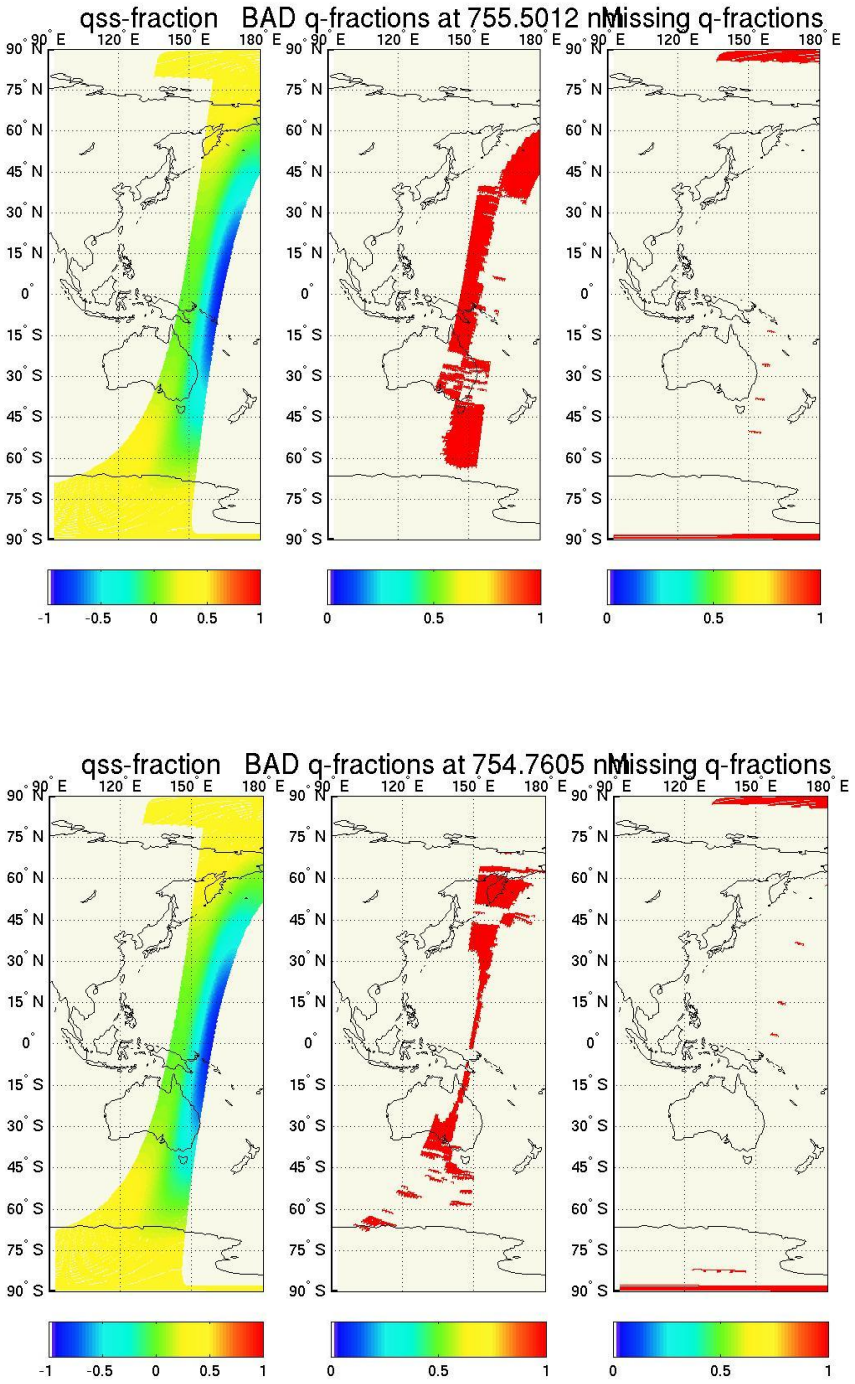

Figure 33: Changes in Stokes fractions flagged as "bad" (middle panels; due to limiting atmosphere criterion) over one orbit. The left panels show the single-scattering equivalent Stokes fraction values and the right panels missing Stokes fractions (e.g. due to increasing signal-to-noise in the polar regions). The results are from PMD bands v1.0 (upper panels) and intermediate band definitions 2.0 (lower panels).

Stokes fractions have been calculated for the test orbits in and after the test upload period and for special geometries only. These special viewing geometries over the orbit are selected as such that the degree of polarisation of the reflected light should be minimal. As a result the derived Stokes fractions should be around zero. Note that only cloud-free situations are taken into account (even though the degree of polarisation for cloudy scenes should also be low, the exact amount of reduction is difficult to quantify) but that other influences from multiple scattering by aerosols etc. can influence the results.

Figure 34 shows Stokes fractions for special viewing geometries again for both cases, employing the old and new band definitions. The processing of the new definitions has also been carried out using the new spectral interpolation scheme. As expected, the results clearly indicate a significant shift towards zero for nearly all wavelengths when employing the new band definitions.

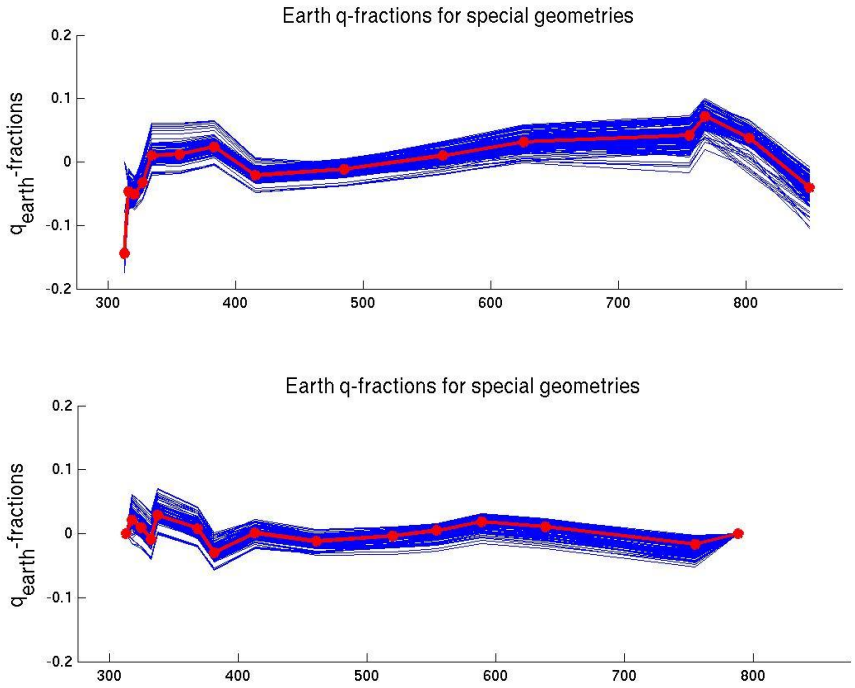

Figure 34: Stokes fractions for special viewing geometries (where q should be close to zero) over one orbit for old band definitions v1.0 (upper panel) and new band definitions v2.0 (lower panel)

Finally, Figure 35 shows the impact on the observed viewing angle dependence for special geometry Stokes fractions. The impact on the latter for changes with respect to band definitions is small. This also points to a more fundamental deficiency in the characterisation of the key-data of the instrument (maybe again linked to zeta). The angular dependence has also been observed in the retrieval of level 2 products and is currently under investigation in the framework of the polarisation study and other initiatives to re-evaluate the key-data accuracy.

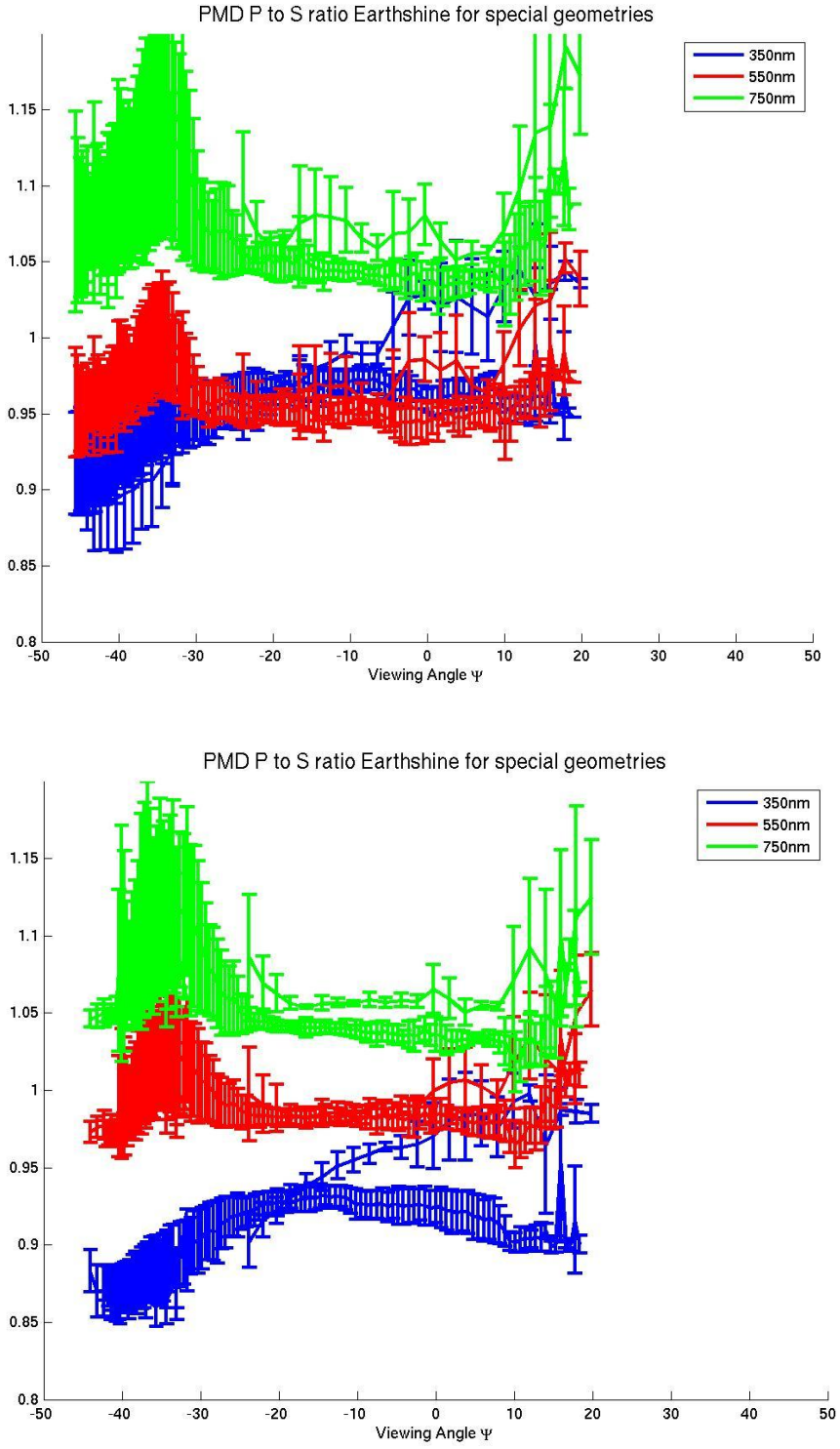

Figure 35: Stokes fractions for special viewing geometries (where q should be close to zero) over one orbit showing dependence on viewing angle of the instrument. Only the mean values are plotted. The error bars indicate the mean distribution (sigma range) over one orbit. The upper panel shows results for old PMD band definitions v1.0. The lower panel indicates results for the intermediate band definitions v2.0.

APPENDIX B LONG-TERM STABILITY OF PMD SPECTRAL CALIBRATION

The long-term stability of the spectral calibration is predominantly influenced by changes in the spectral light source (degradation) and the nominal seasonal (cyclic) and platform (asymptotic) related temperature changes. Long-term temperature changes of both PMD detectors and their influence on the spectral calibration of individual PMDs are accounted for by the daily calibration measurement of the SLS and the cross-correlation algorithm laid out in Section 2.4. However, for some parts of the processing a fixed spectral co-registration of both PMDs is assumed. This holds especially for the PMD band definitions which are uploaded with respect to the PMD detector pixel grid. Any differential changes in PMD detector temperatures between P and S influence the quality of the processing of PMD band data, which cannot be accounted for on-ground. Figure 36 and Figure 37 show the differential changes of the spectral calibration between PMD P and S for one pixel in the IR around 650 nm and the differential change in temperature between both PMDs respectively. The close relation between the long-term behaviour of both curves points to a close link of the differential spectral changes in PMDs with temperature differential change.

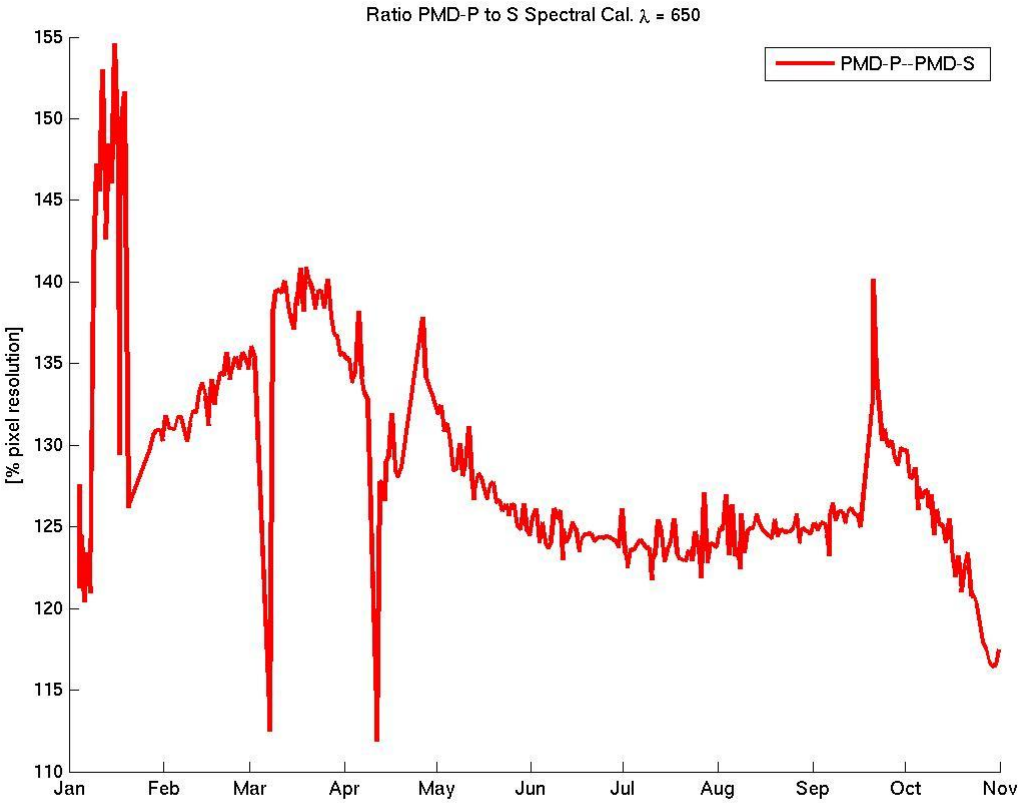

Figure 36: Relative difference in detector pixel fraction between the spectral assignment of one detector pixel around 650 nm for both PMDs S and P (same pixel number) from 1 January 2007 to 1 January 2008. Note that the co-registration shift between S and P is 1 pixel (100%) by default (see Figure 12), i.e. the variation is in sub-pixel range.

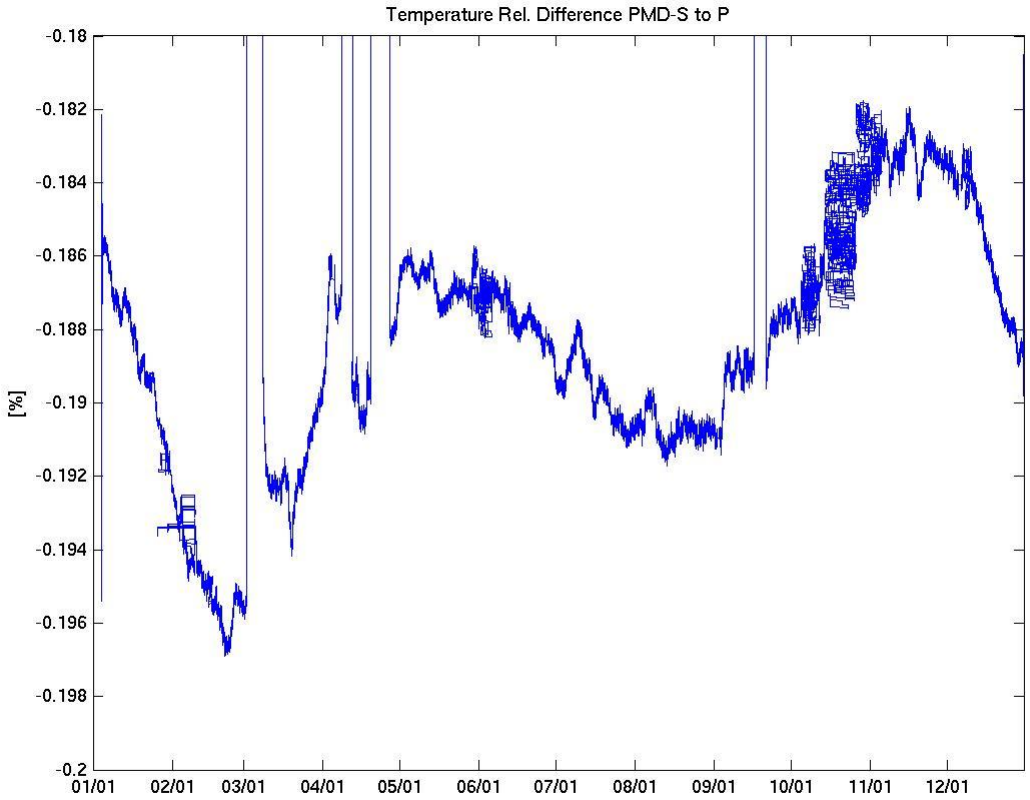

Figure 37: Relative residual between changes in the detector temperature for both PMDs from 1 January 2007 to 1 January 2008

APPENDIX C VIEWING ANGLE DEPENDENCE OF POLARISATION SENSITIVITY TO LINEAR POLARISED LIGHT (χ). IN-FLIGHT DATA MODELLING APPROACH USED FOR PPF VERSION 3.9 TO 4.2.

We expect the observed viewing angle dependence (see Chapter 3) to be related to the key-data characterisation of the angular dependence of the polarisation sensitivity of the detectors to linear polarised light characterised by χ (PGS 6.1 [AD0] 5.2.3). The otherwise quite complex relationship between the signal S_p and S_s from PMD P and S, the Stokes fraction q, and the MMEs (including χ) for PMDs, gets very simple in the case for special geometries for which we assume q=0 (Eq. 229, PGS 6.1 [AD0]):

$$\frac{M_s}{M_P} = \frac{S^S}{S^P} \qquad \textit{Equation 7}$$

Since in this case the relative signal for PMD S to P is a function of α, β, γ (see Section 2.4.2.7) and χ, where χ describes the angular dependence of α and β (note that χ is also used in the derivation of the polarisation sensitivity of FPAs and PMDs to linear polarised light $\mu 2$, [AD0] 5.2.16), we can write Equation 7 as a function of α, β, γ such that

$$\frac{S^S}{S^P} = \frac{\alpha\chi + \gamma}{\beta\chi + 1} \qquad \textit{Equation 8}$$

in the case of special geometries.

C.1 Modelling of χ from In-Flight Data: Approach Applied for PPF 3.9 to 4.2

From this we are able to derive χ from in-flight data fixing α, β, and γ. Since it is clear from Figure 20 that there is an apparent problem in the angular dependence of special geometries and strong variation with wavelength and viewing angle, we make use of PMD raw-transferred measurements taken once per month during the sequence of monthly calibration timelines. For this special timeline PMD data is transferred in full spectral mode (279 spectral read-outs) but with a reduced number of temporal read-outs (only 16 measurements per viewing instead of 256 but taken at nominal PMD integration times 0.0234 sec). PMD raw timelines therefore provide high spectral resolution, however with reduced sampling of the viewing angle. From Figure 20 we expect smooth variation of χ with viewing angle in contrast to a stronger variation with wavelength.

Figure 38 shows the modelled χ for three different wavelengths from 12 RAW orbits taken between January and December 2007. For comparison χ as provided by the current key-data for FM3 has been plotted in dashed lines. The difference between the two sets of data (in-flight versus key-data) already closely resembles the deviation from zero seen in the above Stokes fraction for special geometries plot, especially in the UV and for East viewing geometries.

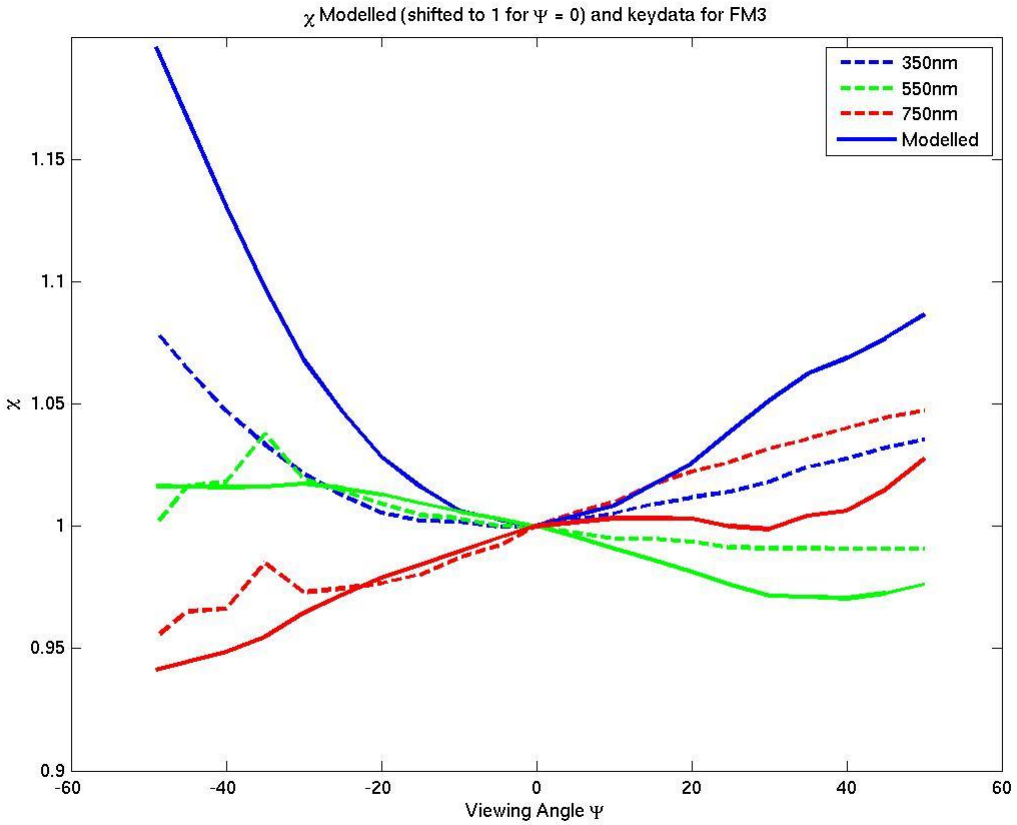

Figure 38: Modelled χ from in-flight data using 12 RAW PMD orbits between January and December 2007. The solid lines show the result for the in-flight modelled data and the dashed lines for key-data values of χ used up to and including processor version 3.8.

Figure 39 shows the 2D surface of χ as derived from in-flight data with respect to wavelength and viewing angle. For internal-viewing geometries, i.e. viewing angles larger than 50 degrees used during calibration measurements (looking at on-board light-sources) the existing key-data values for χ are used. Finally, Figure 40 shows the difference of the 2D surface of χ with respect to the original key-data.

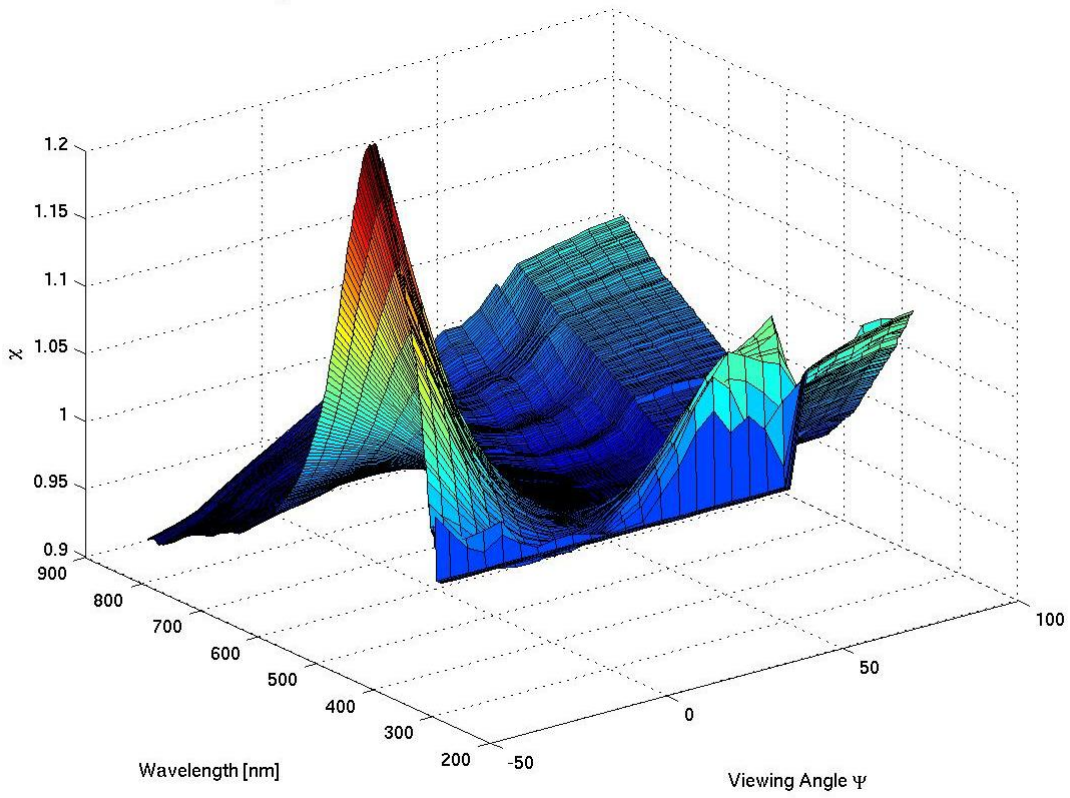

Figure 39: Modelled χ from in-flight data using 12 RAW PMD orbits between January and December 2007 with respect to wavelength and viewing angle. Note that for internal-viewing geometries (> 50 degrees) during calibration measurements, the modelled surface has been merged with the existing key-data values.

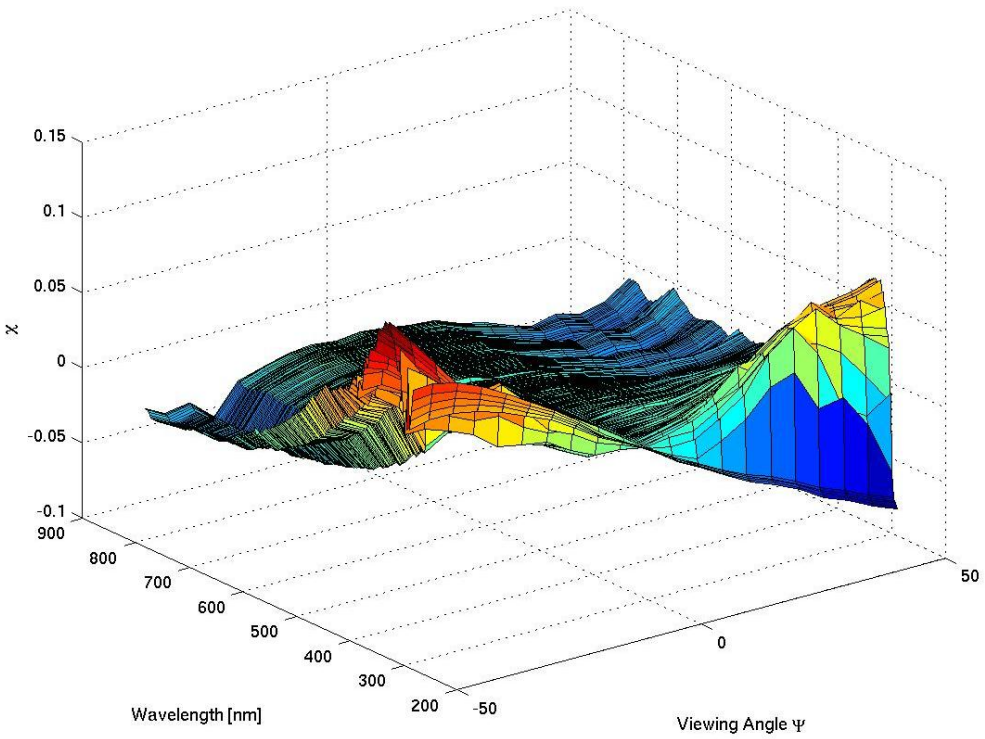

Figure 40: Residual between χ from in-flight and key-data values for viewing geometries < 50 degrees

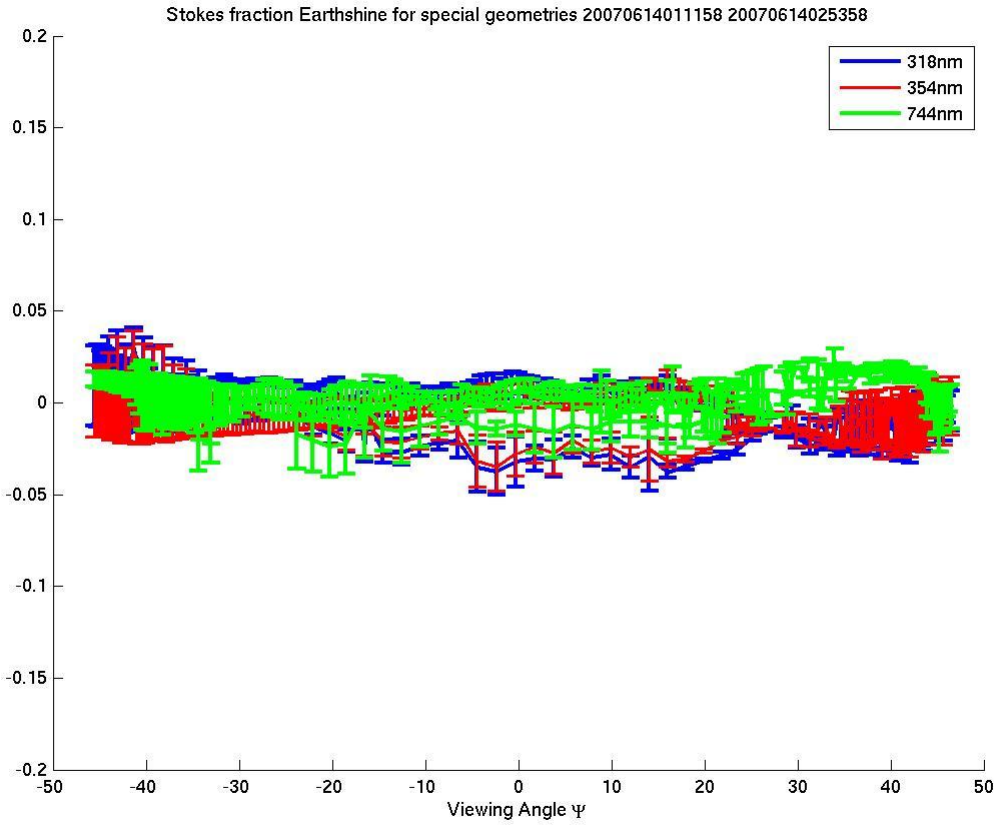

Figure 41: Stokes fractions for special viewing geometries (where q should be close to zero) over one orbit showing dependence on viewing angle. The error bars indicate the 1σ statistics on the mean. Here we use in-flight modelled data for χ.

Note that the angular dependence for radiometric response of PMD (κ for PMD) has been measured on-ground during the calibration campaign only for ambient temperature, resulting in a significant amount of noise on the signal in the UV-to-visible region. The data have therefore not been considered as being of sufficient quality. Instead it has been assumed that the angular dependence of the absolute radiometric response for PMD is the same as for FPA (for which κ actually has been measured).

C.2 Changes Due to the Usage of the Modelled χ Values (PPF 3.9)

During level 0 to 1B correction of radiance data for the degree of polarisation using the derived Stokes fractions, χ is applied in the calculation of the latter based on PMD signals as well as the application of Stokes fraction for the polarisation correction of FPA data (see Eq. 229 and 251 [AD0]). We replace the original key-data file

POL_CHI.203 (for PPF 3.9 activated on 10 March 2008)

with modelled data for χ taken from the grids of PMD data shown above. For all wavelengths (below 300 nm) and viewing angles (above 50 degrees) for which in-flight modelled data are not available, the original data have been used.

C.3 Additional Changes to the Usage of the Modelled χ Values and to α (PPF 4.0 and 4.1)

C.3.1 PPF 4.0 (26 June 2008)

It has been observed that even though the viewing-angle dependence deviation from 0 for special geometry Stokes fractions has significantly improved after applying the new modelled χ values by modifying POL_CHI.203 to both PMD and FPA radiances, a larger viewing-angle dependence for level 2 retrievals, especially in the UV for tropospheric ozone columns, has been observed starting with the installation of PPF 3.9. Figure 42 shows the deviation of tropospheric ozone columns in the tropics for West, nadir and East pixels as retrieved by the operational O3MSAF algorithm (Opera; courtesy O. Tuinder, KNMI) for various level 1B data versions. After the installation of PPF 3.9 the deviation has grown (even though the Stokes fraction quality has improved). Since the modelled χ values are retrieved from PMD signals only, we decided to apply the modelled values for PMD data only and use the original key-data for χ for FPA signal correction. For this we introduced a new key-data set called

POL_CHI_PMD.203 (activated with PPF 4.0 on 26 June 2008),

holding the in-flight modelled χ values, which are applied to PMD signals (i.e. the derivation of Stokes fractions) only.

Note, since χ accounts for the polarisation sensitivity of the viewing mirror to different angles of incident light, the calibration using χ should apply to both FPA and PMD signals. However, the deviations of in-flight modelled χ from its original values may partly be due to other unknown PMD detector-related changes with respect to the on-ground calibration of the instrument.

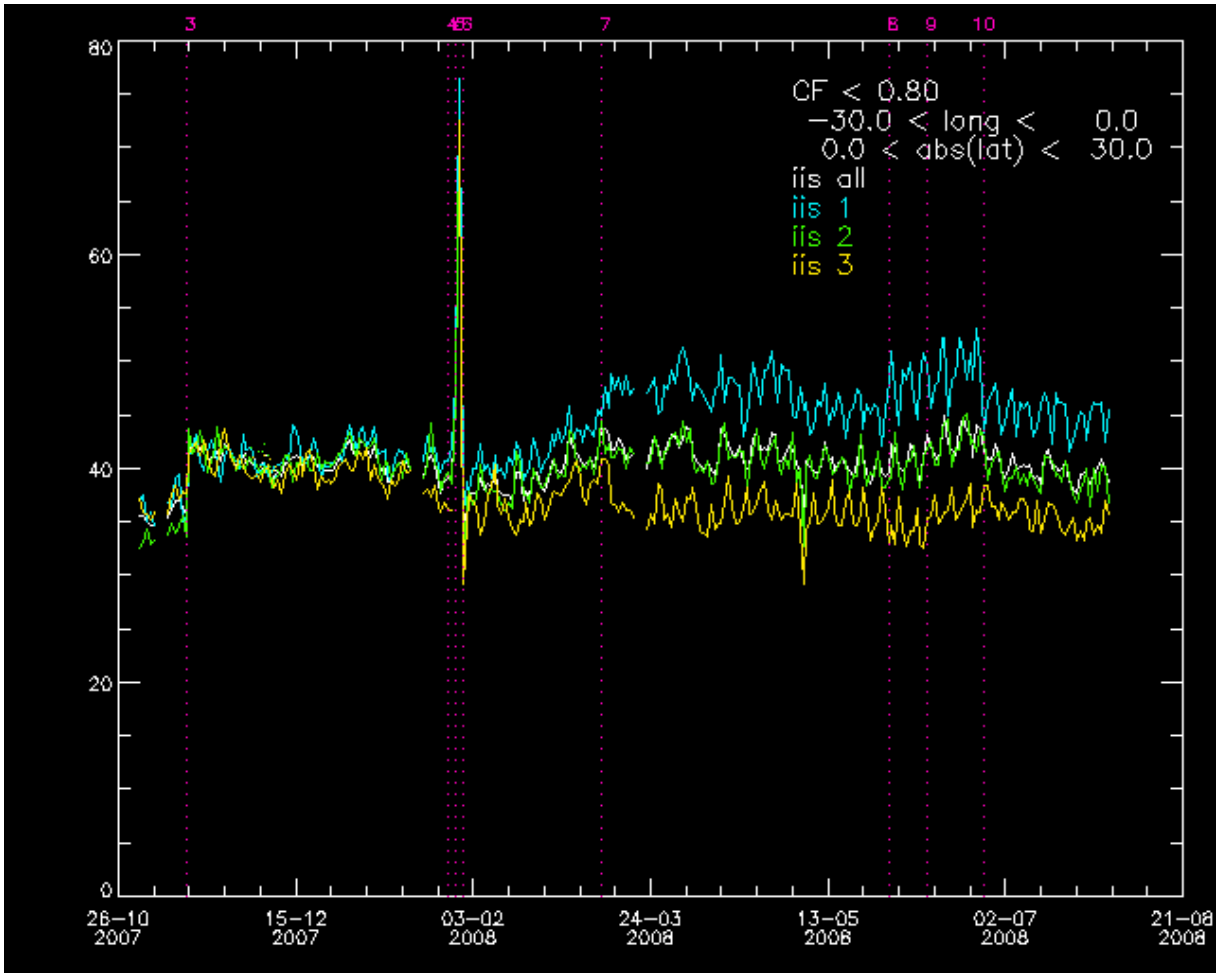

***Figure 42: Time series of sub-tropical tropospheric Ozone columns as derived from the O3MSAF Opera Ozone Profile retrieval algorithm (KNMI/ O. Tuinder). The plot shows the separation of the East (blue), Nadir (green) and West (yellow) ground-track pixels as of the installation of PPF 3.9 with POL_CHI.203 in March 2008, for which the newly modelled χ values are applied to* both *PMD and FPA signals. After the installation of PPF 4.0 at end of June 2008 with the introduction of POL_CHI_PMD.203 (applying the in-flight modelled χ values for derivation of Stokes fractions only) and using the original POL_CHI.203 key-data, the separation has reduced.* Note, that at the same time and for both POL_CH_PMD and POL_CHI key-data sets used, the quality of the Stokes fractions has significantly improved using in-flight modelled data [RD1].**

C.3.2 PPF 4.1 (7 January 2009)

After 26 June 2008 and thanks to the first GOME-2 level 1B reprocessing campaign, 18 months of GOME-2 level 1A and 1B data (G2RP) orbits of raw PMD measurements have became available based on the same processor version 4.0. A re-modelling of χ from in-flight data as described in Section 1.1 has been carried out using the available G2RP data providing a larger data basis. In addition, α has been fitted to the same in-flight data prior to the fitting

of χ using nadir (χ=1) signals only using Equation 8. Subsequently χ has been fitted as previously but with changed α values (Experiment G).

Figure 43 shows the changed values of $\alpha+\gamma$ as a result of a modelled α leaving β and γ unchanged and for χ=1 (nadir only). The modelling of α results in an offset which shifts the subsequently modelled χ values more towards 1 around nadir (Ψ=0) and therefore reducing the overall residual and forced shifting of χ to 1 (see Section 1.1). Additional minor improvements to the modelling code allowed for a larger amount of valid data being accepted for the modelling in addition to the prolonged time-span.

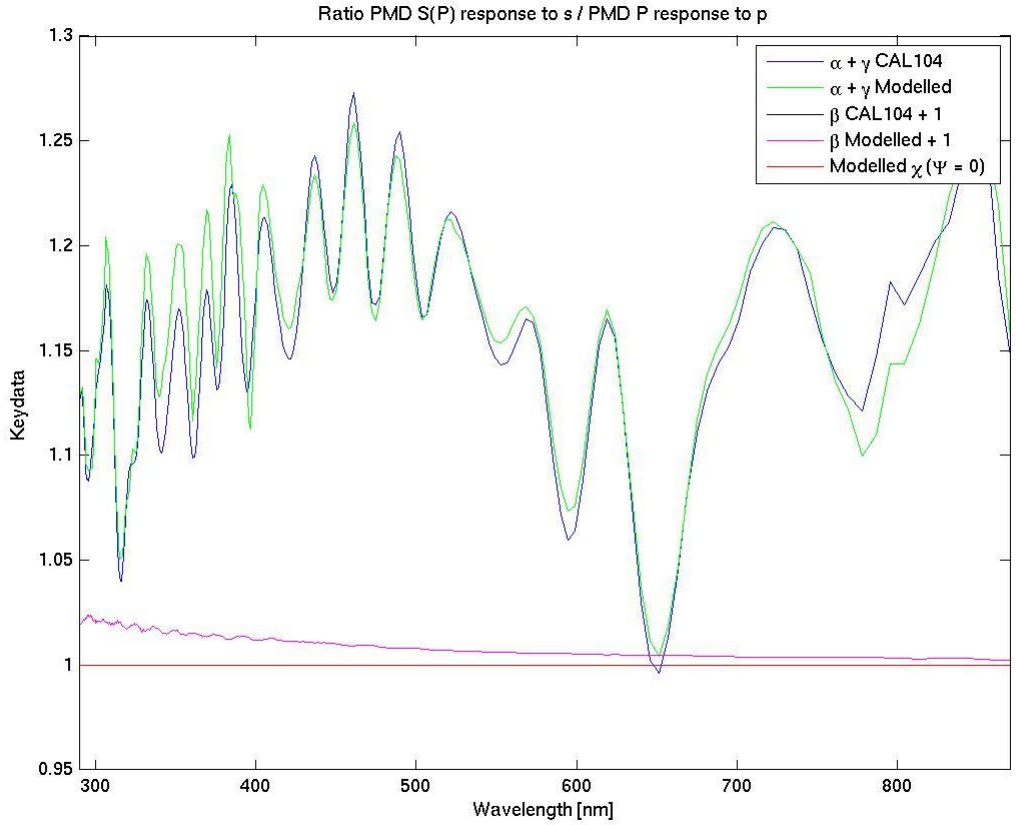

Figure 43: Result of the modelling of α from in-flight data at nadir (Ψ=0) positions for which χ=0. The modelled α values (green line) show a shift with respect to the original values, which (when applied in Equation 8) reduces the shift of modelled χ values at nadir position.

Figure 44 shows the residual in χ between the original key-data and the new modelling results including the newly modelled α and based on 18 PMD raw orbits of reprocessed level 1 data. Largest changes with respect to the previous modelling campaign (cf. Figure 24) are observed in the UV.

As a result of the latest in-flight modelling for PPF version 4.1, the following files have been updated:

POL_CHI_PMD.203 (activated with PPF 4.1 on 7 January 2009)
POL_ALPHA.203 (activated with PPF 4.1 on 7 January 2009).

The improvements to the viewing-angle dependence of Stokes fractions by using the in-flight modelled key-data have been verified by the Polarisation Study Group report issued in December 2008 [RD1].

Overall the impact of this revised modelling of χ on the quality of Stokes fractions, level 1B main channel radiances and level 2 retrievals appears to be small. However, the overall procedure of deriving χ values from in-flight data is now much more robust and consistent.

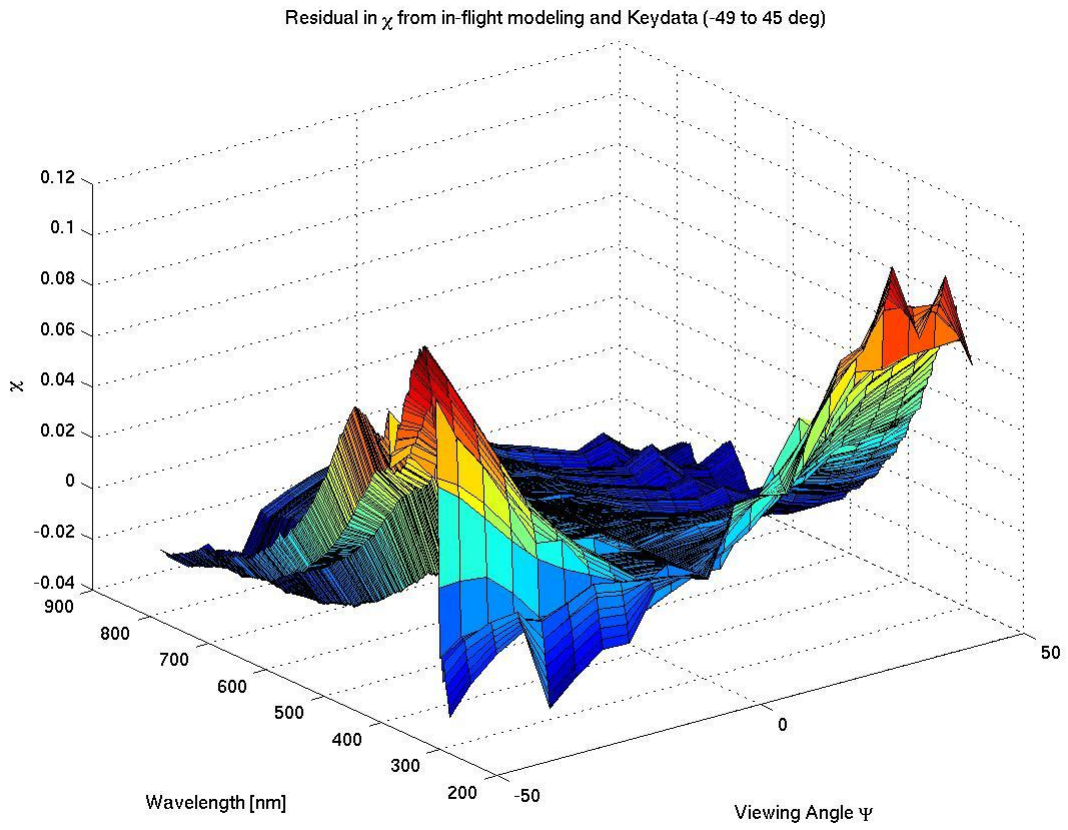

Figure 44: Same as Figure 40 but now for the revised modelling of χ from in-flight data as explained in this section. Note the different scale in the vertical axis with respect to Figure 40.